1993

Toughening mechanisms in a high temperature cyanate ester resin modified with a thermoplastic polyimide

Michael DiBerardino
Lehigh University

AUTHOR:

DiBerardino, Michael

TITLE:

Toughening Mechanisms in a High Temperature Cyanate Ester Resin Modified with a Thermoplastic Polyimide

DATE: October 10, 1993

TOUGHENING MECHANISMS IN A HIGH TEMPERATURE CYANATE ESTER RESIN MODIFIED WITH A THERMOPLASTIC POLYIMIDE

by

Michael DiBerardino

A Thesis

Presented to the Graduate Committee

of Lehigh University

in Candidacy for the Degree of

Master of Science

in

Polymer Science and Engineering

Lehigh University

1993

CERTIFICATE OF APPROVAL

This thesis is accepted and approved in partial fulfillment of the requirements for the Degree of Master of Science in Polymer Science and Engineering

Date 8/19/93

Professor in Charge

Department Chairperson

Polym. Sci. Eng.

ACKNOWLEDGMENTS

I would like to thank my faculty advisor, Dr. Raymond Pearson for his help and advice in the areas of toughening mechanisms and fracture mechanics. I would like to acknowledge Dr. B.T. DeBona of Allied-Signal Inc. and Dr. M.A. Vallance of Ciba-Geigy Corp. for providing the materials used in the study. I would like to thank Mr. Roland C. Cochran of the Naval Air Warfare Center for allowing me to shirk my other responsibilities in lieu of finishing this thesis. I am grateful to Drs. Charles G. Hegedus and Thomas M. Donnellan for their advice and guidance pertaining to my research, career and life in general. Finally I am eternally indebted to my wife, Nicole for her unending support and understanding during this very turbulent period in my life. I once again extend my sincere thanks to all of you.

"The significance of a man is not what he attains but rather what he longs to attain"
- Kahil Gibran

"I count them and recount them. It is difficult. But I am a man who is naturally interested in matters of consequence"
- Antoine de Saint-Exupery
"The Little Prince"

TABLE OF CONTENTS

LIST OF FIGURES

LIST OF TABLES

LIST OF APPENDICES

ABSTRACT

A high temperature phenol triazine resin system has been modified with a high temperature thermoplastic polyimide powder. The phenol triazine (PT) resin (Primaset^{TM}) exhibits a glass transition temperature, Tg, in excess of 400°C and the thermoplastic polyimide (TPI) (Matrimid^{TM} XU218) has a Tg in the range of 320-330°C. Several loadings of TPI were investigated and the effect on morphology, mechanical properties and fracture toughness has been determined. Addition of 21% TPI increased the fracture toughness of the blend 50% while maintaining the temperature and mechanical capabilities of the unmodified PT resin. The objective of this research is to understand the fundamental mechanisms responsible for the improved toughness in high Tg thermosetting polymers modified with a second phase thermoplastic material. Examination of the fractured specimens revealed evidence of both crack bridging and crack tip pinning mechanisms. Application of well-known mechanical models for the two toughening mechanisms were correlated with the experimental results. The correlations indicate that crack tip pinning is the predominate mechanism responsible for the increase in toughness for the PT/TPI system.

1. INTRODUCTION

The use of high temperature polymers has been driven by potential application of these materials in the aerospace industry. Polymers with use temperatures above 300°C have many potential applications as structural adhesives and composite resins in both the military and commercial aircraft offering large weight savings by replacing steel and titanium in airframe structures. In addition to the aerospace industry, thermally stable polymer are finding applications in the microelectronics, and automotive industries. The attractiveness of these polymer systems is their high thermal stability, resistance to oxidative degradation at high temperature, corrosion resistance, dielectric properties, and flame resistance.

Despite their many advantages, the use of high temperature polymers in many of these applications is limited due to the inherent brittleness and low strain to failure of the polymer resins. Because of the brittle nature of these polymers, high temperature composites and adhesives are very susceptible to matrix cracking from thermal cycling or impact damage. The development of high temperature polymer systems with enhanced toughness would increase the current use potential for these materials as structural adhesive and composite resins.

1.1 BACKGROUND

In order to better understand toughening of high temperature polymers, it is useful to review recent work on toughening of brittle epoxy resins. The most common approach to toughening epoxies has been the incorporation of a functionalized rubber such as carboxyl terminated butadienen-acrynitrle copolymers (CTBN). Upon curing, the rubber component forms a dispersed second phase in a continuous epoxy phase. This approach has shown significant improvements in fracture toughness. This toughening mechanism for this type of blend has been shown to be cavitation of the rubber particles and shear yielding of the matrix polymer [1-4]. However, the addition of soft rubbery inclusions into a stiff matrix has its drawbacks. A reduction in use temperature, yield strength and modulus of the polymer is often observed. Furthermore, it has been demonstrated that as the cross-link density of the epoxy increases the glass transition temperature increases but the resin becomes less ductile and the ability of rubber particle to improve toughness is diminished as seen in Figure 1 [5]. Clearly such an approach cannot be taken if tough, high temperature polymers are desired.

Indeed, the highly cross-linked structure of the BMI's and PI's (see Figure 2) that provides the high temperature capabilities also limits their ability to be toughened by

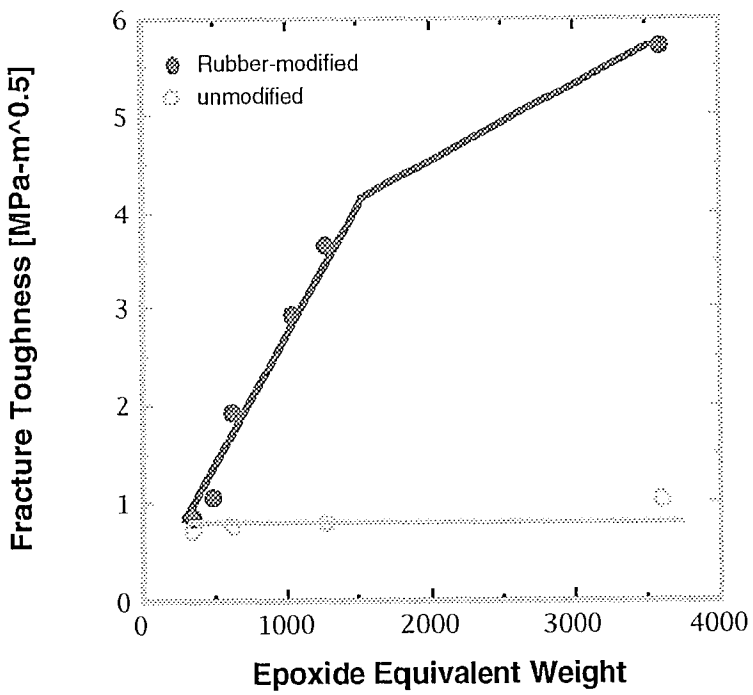

Figure 1. Effect of epoxy crosslink density on rubber toughness. Low crosslinked epoxies show dramatic increase in fracture toughness while high crosslinked epoxies exhibit very little improvement in toughness [5].

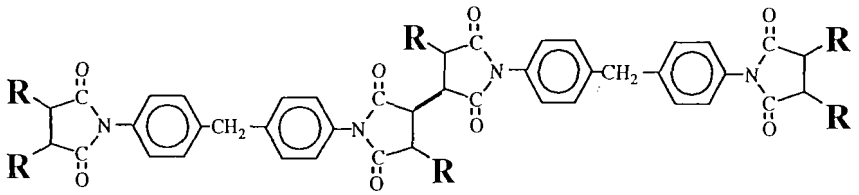

Bismaleimide (BMI)

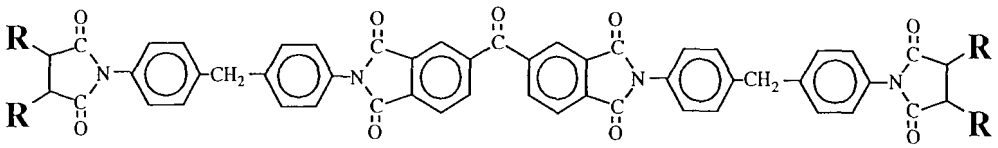

Polyimide (PI)

Figure 2. Chemical structure of Bismaleimide and Polyimide polymers.

elastomeric modifiers. For example, Kinloch and Shaw [6] added CTBN to a bismaleimide polymer (Tg > 250°C) system; significant increases in toughness were not achieved until a rubber concentration of 100 phr. As expected for such a high rubber loading, significant reduction in use temperature and modulus properties were seen. Another example of toughening high temperature polymers by rubber modification was reported by Sachdeva [7]. Sachdeva added rubber as one of several tougheners to polyimide (Tg > 300°C) system. A significant increase in fracture energy (G_{Ic}'/G_{Ic}^{o} = 5) however, with a decrease in Tg of 137°C was reported with an undisclosed amount of toughener. The need for an alternative approach to toughening is evident.

The use of thermoplastic modifiers to brittle polymers offers the potential to provide improved toughness without a decrease in thermal or mechanical properties. In addition, this concept is applicable to highly cross-linked systems that could not be toughened by the addition of rubber particles. Recently several publications have focused on thermoplastic toughening of epoxies [8-16]. The results of these studies are summarized in Table I and discussed below.

Numerous engineering thermoplastics have been employed to toughen epoxies with varying amount of success. The basic chemical structure of these thermoplastics are shown

Table I

Review of improvements in toughness for various thermoplastic modified epoxies

Epoxy Resin	Thermoplastic Modifiers	Toughness Increase	Ref.
DGEBA[1]	Commercial PES	ΔK_{Ic} = 0.2 MPa $m^{1/2}$	[8,9]
DGEBA[1]	PES-OH	ΔK_{Ic} = 0.2 MPa $m^{1/2}$	[13]
DGEBA[1]	PSF-OH, 5300 Mn	ΔK_{Ic} = 0.3 MPa $m^{1/2}$	[10]
	PSF-OH, 8200 Mn	ΔK_{Ic} = 0.2 MPa $m^{1/2}$	
DGEBA[1]	PFS-NH_2, 5300 Mn	ΔK_{Ic} = 0.2 MPa $m^{1/2}$	[11]
	PFS-NH_2, 36500 Mn	ΔK_{Ic} = 0.6 MPa $m^{1/2}$	
	PEK-NH_2, 6980 Mn	ΔK_{Ic} = 0.2 MPa $m^{1/2}$	
	PEK-NH_2, 17800 Mn	ΔK_{Ic} = 2.0 MPa $m^{1/2}$	
DGEBA[2]	Commercial PPO	ΔK_{Ic} = 0.9 MPa $m^{1/2}$	[15]
	Commercial PPO-PDMS	ΔK_{Ic} = 0.9 MPa $m^{1/2}$	
TGDDM[3]	PES	ΔK_{Ic} = 0.2 MPa $m^{1/2}$	[12]
TGDDM[3]	PES-OH	ΔK_{Ic} = 0.5 MPa $m^{1/2}$	[13]
TGDDM[3]	Commercial PEI	ΔK_{Ic} = 0.5 MPa $m^{1/2}$	[14]

[1]DGEBA/DDS system, Tg ≈ 210°C, K_{Ic} ≈ 0.8 MPa $m^{1/2}$

[2]DGEBA/PIP system, Tg ≈ 90°C, K_{Ic} ≈ 0.8 MPa $m^{1/2}$

[3]TGDDM/DDS system, Tg ≈ 230°C, K_{Ic} ≈ 0.6 MPa $m^{1/2}$

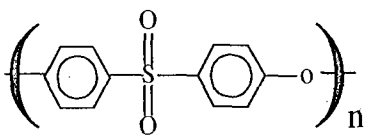

Poly(ether sulfone) (PES)

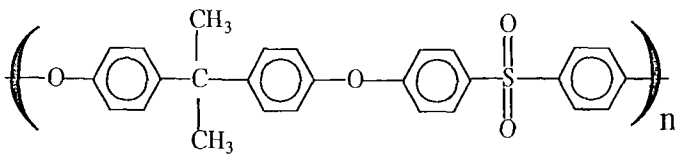

Polysulfone (PSF)

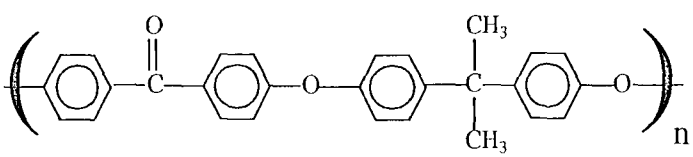

Poly(arylene ethr ketone) (PEK)

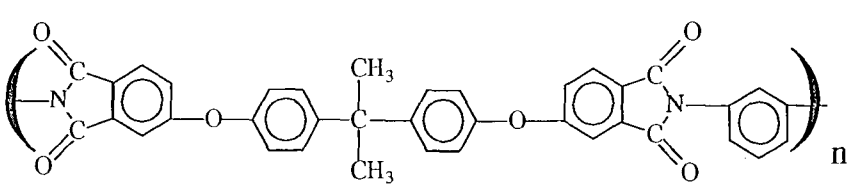

Poly(ether imide) (PEI)

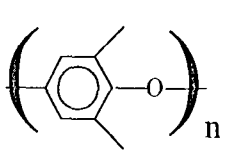

Poly(phenylene oxide) (PPO)

Figure 3. Chemical structure of thermoplastic modifiers.

in Figure 3. In the early 1980's, Bucknall and Partridge [8] and Raghava [9] both attempted to toughen epoxy resins with a commercial polyethersulfone (PES), Vitrex™. The resulting increase in fracture toughness was minimal in spite of the existence of phase separated PES particles ΔK_{Ic} = 0.2 MPa$m^{1/2}$. Poor adhesion of the matrix resin to the thermoplastic particles was cited as a possible reason for the lack of toughness improvement.

Hedrick et al. [10,11] and Cecere and McGrath [12] incorporated thermoplastic modifiers with reactive end-caps into a diglycidyl ether of bisphenol-A (DGEBA) epoxy resins. The base epoxy resin is shown in Figure 4. Hedrick [10] used hydroxy-functionalized poly (aryl ether sulfones) PSF with varying molecular weights to improve the toughness of epoxy resins. The results form this study showed that addition of functionalized PSF produced a particulate two phase morphology with particle size increasing with molecular weight. The fracture toughness of the system also increased as a function of the molecular weight of the thermoplastic with a maximum increase in K_{Ic} of 0.7 MPa $m^{1/2}$. Hedrick attributed the success of the functionalized thermoplastic tougheners to the strengthened interface. Cecere [12] use amine-functionalized PSF and poly (ether ketone) PEK with varying molecular weights to modify the same epoxy. The results of this studies were similar, for both modifiers the toughness increased as a function of

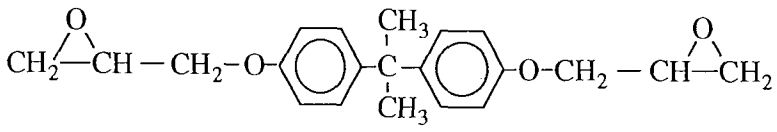

DGEBA epoxy resin

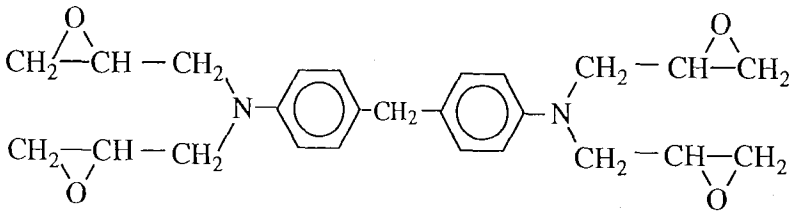

TGDDM epoxy resin

Figure 4. Chemical structure of DGEBA and TGDDM epoxy resins.

molecular weight. Of the two thermoplastics materials, the PEK (ΔK_{Ic} of 1.4 MPa $m^{1/2}$) provided better toughness enhancement than the PSF (ΔK_{Ic} of 0.6 MPa $m^{1/2}$). The improved toughness seen in this study was attributed to the increased ductility of the high molecular weight thermoplastics.

Raghava [13] investigated the effect of functionalized PES on a tetraglycidyl 4,4'-diaminodiphenyl methane (TGDDM) epoxy systems and Fu and Sun [14] studied the effect of hydroxy-functionalized PES on a DGEBA epoxy systems. The base tetrafunctional epoxy resin is shown in Figure 4 As in the previous work on non-functionalized PES, ΔK_{Ic} of 0.2 MPa $m^{1/2}$. These results indicate that the used of reactive ends did not significantly improve the fracture toughness of PES modified systems. Fu [14] also investigated hydroxy functionalized PSF with a TGDDM epoxy with a substantial improvement in toughness ΔK_{Ic} of 0.5 MPa $m^{1/2}$. The lower elongation to failure of the PES was cited as the reason for the lack of toughness enhancement.

Bucknall and Gilbert [15] used a commercial polyether imide (PEI), Ultem™ 1000 resin, to toughen a TGDDM epoxy system. The PEI separated into second phase particles with increasing particle size for increasing amount of added thermoplastic. The authors show a linear increase in fracture toughness with volume fraction of PEI to a maximum

of ΔK_{Ic} of 1.0 MPa $m^{1/2}$ for 16.6% volume PEI. These results are significant in that the use of a nonreactive thermoplastic provided a significant increase in fracture toughness.

Pearson and Yee [16] use several commercial thermoplastics to toughen a DGEBA epoxy resin. Their results indicate that phase separation is necessary for toughness increase. In addition, resins modified with poly (phenylene oxide) PPO and a poly(ether imide - dimethyl siloxane) random copolymer gave significant increases in toughness (ΔK_{Ic} of 1.0 MPa $m^{1/2}$) for both modifiers. The authors suggested that smaller particles provide more toughness that larger particles and that microcracking provides the toughening mechanism.

The concept of toughening epoxy resin with thermoplastic has been extended to toughening bismaleimide (BMI) and polyimide (PI) resins. Initial attempts by Lin et al. [17] at modifying BMIs with thermoplastics concentrated on commercially available nonreactive materials such as polyetherimide, polyethersulfone. The results of these experiments show considerable increase in fracture toughness, ΔK_{Ic} between 0.6 and 0.7 MPa $m^{1/2}$ for various loadings of PEI. The blends modified with PES did not show as dramatic an increase, ΔK_{Ic} = 0.23 MPa $m^{1/2}$. The results

for PES modified BMI are similar to those found for PES modified epoxy systems [8,9,12,13].

Stenzenberger et. al. [18] modified BMI with reactive and nonreactive poly(arylene ethers) (PAE). The effect of molecular weight on toughness was studied for each of three endcaps, floro-terminated (nonreactive), allyl-terminated, and maleimide-terminated (reactive). In general these results indicated and change in morphology and an increase in toughness with molecular weight. All systems displayed an increase in particle size with increasing molecular weight, the floro-terminated PAE exhibited phase inversion at the highest molecular weight. For the nonreactive thermoplastic, only the phase inverted system gave significant increase in toughness, while the both reactive PEA's showed improvements in toughness for all molecular weights. The authors describe good adhesion for all end capped PEA's as determined by SEM examination of the fracture surface.

Wilkinson et. al. [19] also investigated the effect of molecular weight for reactive and nonreactive poly(arylene ether sulfone) modified BMI's. These results showed similar trends to Stenzenberger, toughness increases and molecular weight increases. The authors describe various morphologies that occur but are unable to discern which one provide the optimum toughness. The thermoplastic containing reactive

end groups showed a greater improvements in fracture toughness than the thermoplastic containing nonreactive end groups. BMI resins with amine and maleimide end capped PAEs showed a ΔK_{Ic} of 1.0 MPa $m^{1/2}$, while the increase for the nonreactive phthalimide end capped PAEs was ΔK_{Ic} = 0.3 MPa $m^{1/2}$. The authors claim the reactive end groups provide better interphase adhesion. Although there is no direct evidence of this, certainly reaction of the thermoplastic into the continuous BMI phase provide improved environmental and solvent resistance.

Johnston et. al. [20] used a commercial thermoplastic polyimide to toughen a thermosetting polyimide composite matrices. The thermoplastic powder was metered on the carbon fiber prepreg toe to toughen the interply region of the composite laminate. The results of this study showed an increase in interlaminar fracture energy. G_{Ic}'/G_{Ic}^{o} = 1.22 and G_{IIc}'/G_{IIc}^{o} = 1.18. The authors described a single phase morphology with a T_g slightly lower than either the unmodified resin or the thermoplastic modifier. This would suggest that the thermoplastic acted as a chain extender to reduce the crosslink density and enhance the toughness.

As described above, there has been a great deal of work investigating the toughness improvements associated with various thermoplastic/thermoset blends. Despite the vast amount of effort spent on trying to improve toughness, a

clear understanding of the parameters associated with thermoplastic modified thermosets has not been established. A determination of the influences of the parameters and the mechanism responsible for increase toughness must occur before the optimum design can be achieved. To understand the influence of various parameters on toughness enhancement, a discussion of several toughening mechanisms will follow.

1.2 TOUGHENING MECHANISMS

1.2.1 Crack Bridging Model

Enhanced toughness due to crack-bridging has been sighted as a mechanism for rubber, glass sphere, and thermoplastic modified polymer systems [10-14,16]. The proposed role of the modifier is to span the crack surfaces in the crack wake and apply compressive traction inhibiting crack opening. This effectively reduces the applied stress intensity at the crack tip. Alternatively, the increase in toughness can be attributed to the energy required to plastically deform (stretch) and tear the bridging particles. Plastic deformation of the particles in the material surrounding the crack tip can provide additional crack shielding. A schematic diagram of crack bridging mechanism is shown in Figure 5.

Crack bridging models have been presented by Ahmad [21]

and Kunz-Douglas [22,23] for rubber modified epoxy resins. The crack bridging models emphasize the strength of the rubber particle in the epoxy matrix whereby the increase in toughness is attributed to the stretching and tearing of the particles in the crack wake. Quantitatively these models relate increase in toughness to particle size, particle stiffness and tear energy in the following manner:

$$\frac{K_{Ic}'}{K_{Ic}^{o}} = \phi\ (1 - V_f) + \frac{V_f\ E^*\ \Gamma_t}{2\ \phi\ (1 - V_f)\ K_{Ic}^{o2}} \qquad (1)$$

where K_{Ic}' is the fracture toughness of the modified resin.

K_{Ic}^{o} is the fracture toughness of the unmodified resin.

ϕ is a correction factor that accounts for crack bowing.

V_f is the volume fraction of rubber particles.

Γ_t is the tearing energy of the rubber particles.

E^* is the stiffness of the rubber particles.

The crack bridging models predict that larger particles will provide greater total tear energy consumed by the system and thus enhanced toughness. In addition, increases in the particle stiffness and the tear energy will also result in increased toughness. Although the principal toughening mechanism for rubber modified epoxies has been shown to be rubber cavitation and resin shear yielding [1-4], evidence of particle bridging has been reported particularly for larger particle sizes [24].

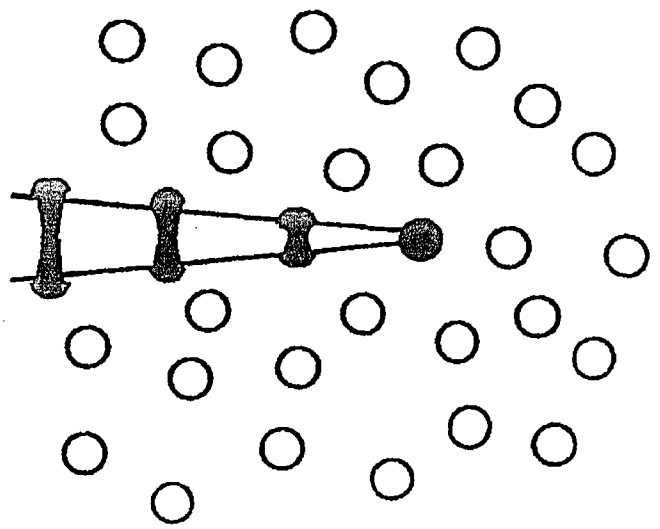

Figure 5. Schematic representation of Crack Bridging model includes particle stretching and spanning the advancing

Rose [25] used a crack bridging model to describe the increase in toughness associated with the addition of glass spheres to an epoxy resin:

$$\frac{K_{Ic}'}{K_{Ic}^{o}} = \frac{[(2s/\lambda) + (2r/\lambda)(K_L/K_{Ic}^{o})^2]^{1/2}}{F_1} \qquad (2)$$

where K_{Ic}' is the fracture toughness of the modified resin.

K_{Ic}^{o} is the fracture toughness of the unmodified resin.

- $2s$ is the surface-to-surface obstacle spacing.
- $2r$ is the diameter of the particles.
- λ is the center-to-center obstacle spacing.
- K_L is the limiting stress intensity factor that specifies the failure of the trailing end of the reinforced zone.
- F_1 is an interpolating function to reproduce the corrected asymptotic expansions for soft springs.

This model emphasizes the ability of the particles to bow the crack front and act as springs to keep the crack surfaces closed. Rose attempts to explain the maxima in fracture toughness as a function of filler content that is often seen in glass filled epoxies. The model proposed relates the ease of fracturing or circumventing the second phase relative the matrix to the increase fracture toughness. The good fit of the model to experimental data appears to support the validity of this model.

Toughening of brittle matrices by ductile particles has been modeled by Sigl [26]. According to this model, two

mechanisms are involved in providing increased toughness, particle bridging that applies compressive traction in the crack wake and particle plastic deformation in the material surrounding the process zone that provide crack shielding. The former mechanism relates improved toughness to increased work to rupture the particle and large particle size, while the latter relates increased toughness to increased yielding due to smaller particles with lower yield strengths. Sigl contents that the crack bridging is the dominant mechanism for improving toughness and the crack shielding from particle yielding is negligible.

Although these models were developed for to describe improvements in toughness for different material systems they all use a similar approach, relating the size of the ligament zone behind the crack tip to the measured toughness. The conclusion of these models is that toughness by crack bridging can be increased by particles with larger size and increased resistant to rupture.

As mentioned previously crack bridging has been proposed as the mechanism responsible for increase toughness associated with thermoplastic modified thermosets [10-14,16]. This is usually based on SEM analysis of the fracture surface showing ductile tearing of the thermoplastic phase material. In addition, several authors have shown that increasing particle size or increasing

molecular weight of the particles (increasing the elongation to failure) provides improved toughness [10,11,16].

1.2.2 Crack Pinning

Crack pinning has also been suggested as a toughening mechanism for rigid inclusions in a brittle matrix [27]. Evidence of crack pinning has been presented for thermoplastic toughened thermoset systems base only on features of the fracture surface [13]. In this mechanism, the moving crack front is impeded when interacts with a rigid or impenetrable second phase material. The front is pinned at the location of the particles causing the crack to bow out between them. Both the change in the shape and length of the crack front will require more energy to propagate the crack. A schematic diagram of crack pinning mechanism is shown in Figure 6. Although frequently cited as a contributing toughening mechanism in thermoplastic modified epoxies, the majority of the modeling of crack pinning has been done on glass-filled epoxy systems [28-31].

Lange [28] modeled the increase in toughness due to crack pinning as a function of the spacing between the particles and the energy required to form a new (larger) surface area. Thus as the distance between the particles decreases and the length of the crack increases, the fracture toughness increases.

$$G_{Ic}' = G_{Ic}^{o} + 2T/d_s \qquad (3)$$

where G_{Ic}' is the fracture energy of the modified resin.
G_{Ic}^{o} is the fracture energy of the unmodified resin.
T is the line tension.
d_s is the center-to-center particle spacing.

Evans [29] extended the model for crack pinning to account for the interactions of neighboring crack segments in an attempt to fit the nonlinear relation between fracture toughness and volume fraction seen by Lange and Radford [31]. Based on considering the crack front to be an array of co-planar semi-elliptical flaws, the overall increase in toughness will be less than predicted by Lange.

$$\frac{K_{Ic}'}{K_{Ic}^{o}} = \left[\left(\frac{\pi}{(2 + d_p/C)}\right)^{1/2}\left[\tan\left(\frac{\pi}{(2 + d_p/C)}\right)\right]^{-1/2}\right] \qquad (4)$$

where K_{Ic}' is the fracture toughness of the modified resin.
K_{Ic}^{o} is the fracture toughness of the unmodified resin.
2C is the surface-to-surface particle spacing.
d_p is the particle diameter.

Green [30] modified these models to account for particle shape and penetrable objects leading to a further reduction in predicted toughen improvement. These three models calculate toughness as a function of volume fraction and independent of particle size. Data presented by Lange and Radford [31] for an epoxy-alumina trihydrate system

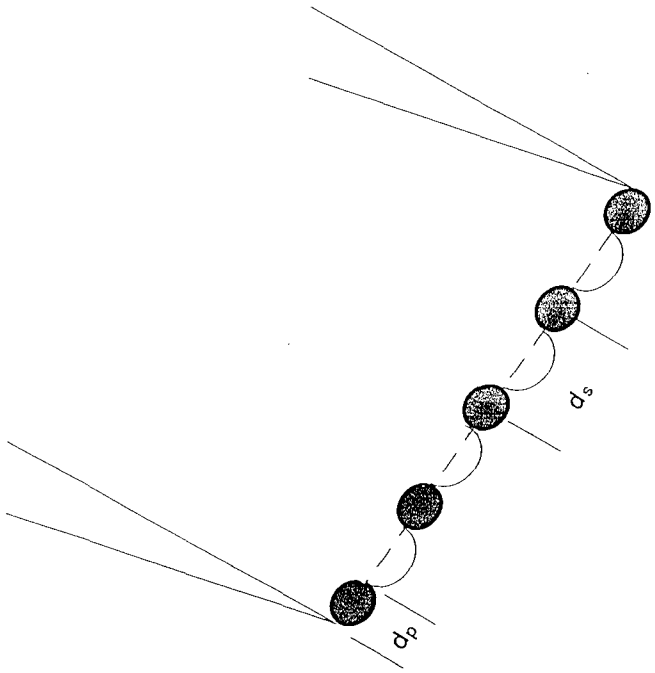

Figure 6. Schematic representation of crack pinning model showing the crack tip being "pinned" by the rigid particles and the crack front "bowing" between the particles

demonstrates that for a constant volume fraction, the fracture toughness increases as the particle size increases. This is due to the larger particles increasing the amount of crack front bowing between the particles and large separations between crack segments.

Evidence for crack pinning mechanism in thermoplastic toughened thermosets has been presented by several investigators [13,14]. This evidence is based primarily on the existence of "tails" near the particles on the fracture surface when examined by SEM. Micrographs of crack front bowing between particles in glass filled epoxies systems has also been presented [27].

1.2.3 Crack Path Deflection

Rigid second phase particles near the tip of the propagating crack can perturb the crack by bowing due to pinning or by crack deflection. Crack path deflection is also a possible mechanism for toughness enhancement in thermoplastic modified thermosets. Crack path deflection arises when interaction between the particle and the crack produces a nonlinear crack front. This deviation causes an increase in the surface area as well as a decrease in the mode I crack opening component. The result of this is an increase in the fracture toughness of the material.

Faber and Evans [32] modeled the increase in toughness due to crack path deflection based on deflection induces reduction in crack driving force. The nonplanar crack is caused by a residual stress or weak a interface. The direction of the deflection depends on this type of residual stress, a compressive strain near the interface will divert the crack around the particle while a tensile strain near the interface will cause the crack to deflect toward the particle. Their analysis shows that the increase in toughness depends only on volume fraction and particle shape and is insensitive to the particle size.

for spheres

$$G_{Ic}' = (1 + 0.87\ V_f)G_{Ic}^{o} \qquad (5)$$

where G_{Ic}' is the fracture energy of the modified resin.
G_{Ic}^{o} is the fracture energy of the unmodified resin.
V_f is the volume fraction of particles.

for rods

$$G_{Ic}' = (1 + V_f(0.6+ 0.007(h/r) - 0.001(h/r)2)G_{Ic}^{o} \qquad (6)$$

where h is the rod length.
r is the rod radius.

for discs

$$G_{Ic}' = (1 + 0.56\ V_f(r/t))G_{Ic}^{o} \qquad (7)$$

where r is the disc radius.
t is the disc thickness.

Rod shaped particles with high aspect ratios provided the most effective toughening followed by disc shaped and

spherical particles respectively. Indeed, for a thermoset modified with spherical particles shows only minimal improvement in toughness. It is unlikely that crack path deflection could be the sole toughening mechanism, more likely the process contributes only modestly to the overall improvement in fracture toughness. In fact the authors suggest that crack pinning and crack path deflection occur simultaneously, although no attempt has been made to combine these models.

1.2.4 Microcracking

An alternate source of toughness could be microcracking of the resin due to the presence of the second phase material. Brittle materials often exhibit microcracking, and microcracking in regions of stress concentrations or at the tip of a crack may postpone the onset of unstable crack growth. Several models have been developed to estimate the contribution of microcracking on the overall fracture toughness [33-38]. These models have been developed primarily for ceramic materials but they may be helpful in understanding microcracking induced toughness in brittle polymers.

The presence of a microcrack zone at the tip of a crack increases the fracture toughness of the materials by reducing the stresses at the tip. This is analogous to the crack tip plastic zone in ductile materials. The reduction

in stresses at the crack tip is due to the increased compliance of the material due to the presence of microcracks. A schematic diagram of microcrack toughening is shown in Figure 7. The net toughness enhancement due to this frontal process zone is not as substantial as predicated by the models due to the counteracting damaged produced by the microcracks and the corresponding reduction in crack extension resistance [35]. The presence of microcracks in the crack wake has been shown to provide additional shielding [34].

Several models employ the use of a saturation state in which the formation of microcracks ceases. This saturation state defines the compliance contribution to the decrease in stress at the crack tip. The saturation state will be reached when the sites for microcrack nucleation become exhausted, thus the toughness can be related to the number and size of the second phase included materials. Evans [36,37] modeled the increase in toughness due to debonding of particles in ceramics and for weakly bonded glass spheres in an epoxy resin. These analyses showed that the toughness was related to the size and distribution of sizes of the particles, the crack propagation resistance of the interface and the elastic moduli, and particle shape. In general smaller particles size with a narrow distribution provided the largest improvement in toughness. Gao [38] in his model extended the relation of toughness to the density of

microcracks to include the effect of crack branching. Application of this model gives reasonable agreement to the increase in toughness due to microcracking in PPO modified epoxies [16].

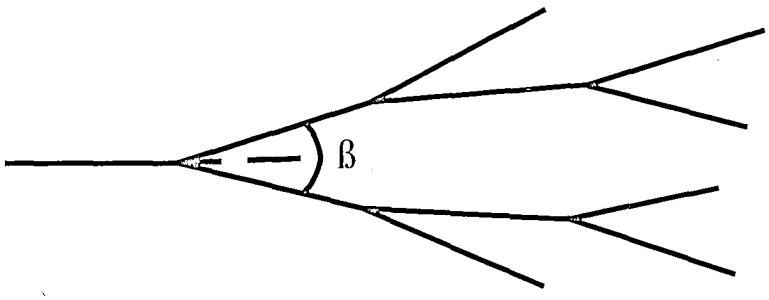

Figure 7. Schematic representation of Microcracking model showing bifurcation of the crack to form multiple surfaces and crack paths (38).

1.3 OBJECTIVE

The objective of the research is to understand the fundamental mechanisms responsible for improvement in toughness in a high temperature thermosetting polymer modified with second phase thermoplastic material. A crosslinked phenolic triazine (PT) resin modified with a thermoplastic polyimide (TPI) was tested to characterize the morphology, mechanical properties and fracture toughness. These tests include: Dynamic Mechanical Analysis (DMA), compression tests, flexural tests, compact tension fracture toughness tests, and Scanning Electron Microscopic analysis.

The fracture surfaces were examined to identify possible mechanisms responsible for increasing the fracture toughness seen on the PT/TPI system. Previously develop mechanical models for the toughening mechanisms identified were correlated to the experimental results. Finally, the contributions of the various mechanisms were assessed in terms of the toughness seen in the PT/TPI system.

2. EXPERIMENTAL

2.1 MATERIALS

The thermosetting resin used throughout this work was Allied Signal's Primaset™ phenolic triazine (PT) resin. The basic backbone of the PT resin is similar to a phenolic novalac resin but with a cyanate (-C≡N) substituted for the hydroxide group (-OH). This substitution produces a cyanate ester oligomeric structure as the precursor to the cured, cross-linked PT resin. The PT resin cross-links through the thermal cyclotrimerization of the cyanate ester groups, producing the triazine linkage [39] as seen in Figure 8.

The phenolic triazine resin was chosen for this study because of its processing characteristics, and thermal properties. The PT resin has a low melt viscosity, 200 cps and 200°C. This is due to the absence of hydrogen bonding that occurs in the phenolic systems. The triazine ring formation is not a condensation type reaction and therefore produces no volatiles. These provide epoxy-like processing capabilities not normally associated with polymers with Tg's above 300°C. The thermal stability of the resin is derived from the triazine ring linkage, which is much more stable than the methylene bridges formed with conventional phenolics.

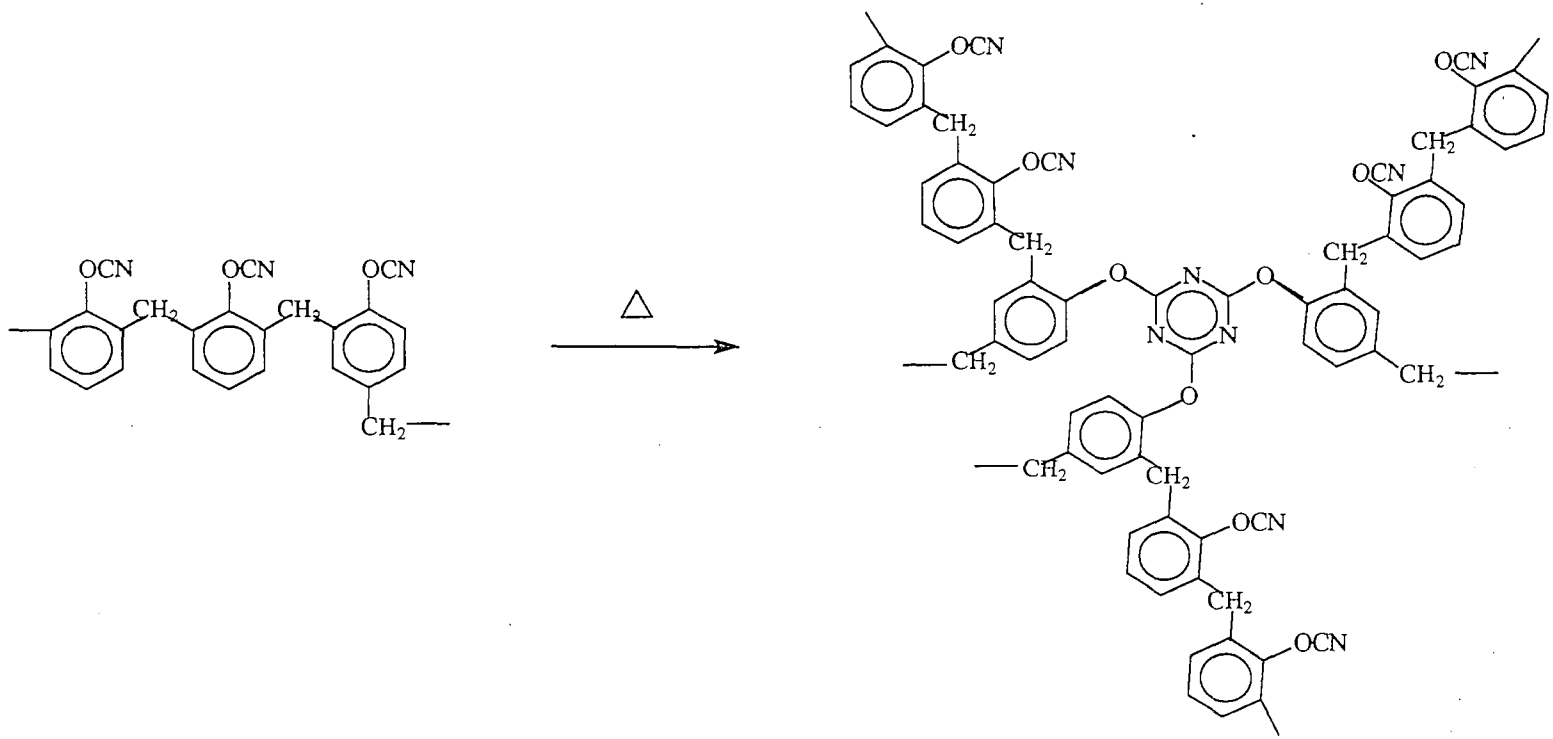

Figure 8. Proposed crosslinking reaction of PT resin

Recent research has shown some success at toughening cyanate esters using thermoplastic modifiers [40]. The thermoplastic component used to toughen the phenolic triazine in this work was Ciba Geigy XU218 resin, a thermoplastic polyimide (TPI). This material is a fully imidized high molecular weight thermoplastic polyimide that provides good toughness and excellent thermal properties [41]. This material was received as a coarse powder with a particle size greater than 200 microns. The TPI was ground down to a fine powder by milling in a ceramic ball mill in a water slurry for three days. The resulting slurry was then dried to 16 hours at 150°C under 760 mm Hg. The powder was separated through USA Standard Testing Sieve Trays. 100% of the powder used was less than 74 microns as measured by the sieve size. SEM micrographs (see Figure 9) show the majority of the particles sizes to range from approximately 50 microns to less than 5 microns.

2.2 MIXING

Five toughener loading levels of TPI were examined in this study, 0%, 5%, 9%, 15%, and 20% by weight. These loading levels correspond to volume fractions of 0%, 5%, 10%, 16%, and 21% respectively. Calculations for volume fractions were made using a resin specific gravity of 1.29 [42] and a 1.2 for the thermoplastic component [41]. These blends were prepared using the following procedure: The

Figure 9. SEM micrograph of TPI particles revealing flake-like particles ranging in size from 50 µm to less than 10 µm.

thermoplastic powder was first dried for 16 hrs at 180°C under vacuum. The resin was heated to 80°C in an oil bath to reduce the viscosity. When the resin reached 80°C, the powder was added and mixed thoroughly with a mechanical mixer for 20 minutes. Resin compositions containing 16 and 21% thermoplastic were too viscous to mix mechanically, these batches were mixed by hand for 30 minutes until the powder was well dispersed.

The TPI thermoplastic powder was not soluble in the PT resin, but it did exhibit some degree of compatibility in that it remained well dispersed throughout the cure this can be attributed in part to the similar specific gravities, 1.26 for the liquid resin and 1.2 for the thermoplastic powder. Two additional thermoplastic modifiers were examined, polyetherimde (PEI) and a polyphenylene sulfone (PPS). Both these modifiers were incompatible with the resin and would not remain dispersed.

2.3 PROCESSING CONDITIONS

After mixing, the PT/TPI resin blends were transferred to a preheated rectangular silicone mold with the inner dimensions (90 mm X 64 mm X 9.52 mm). The resins were degassed in the mold between 120°C and 150°C and subsequently cured for 2 hrs at 200°C. The cured resin plaques received a free standing post cure with dwells at 100°C, 150°C, 200°C, 250°C and 300°C for a total of 6 hrs as

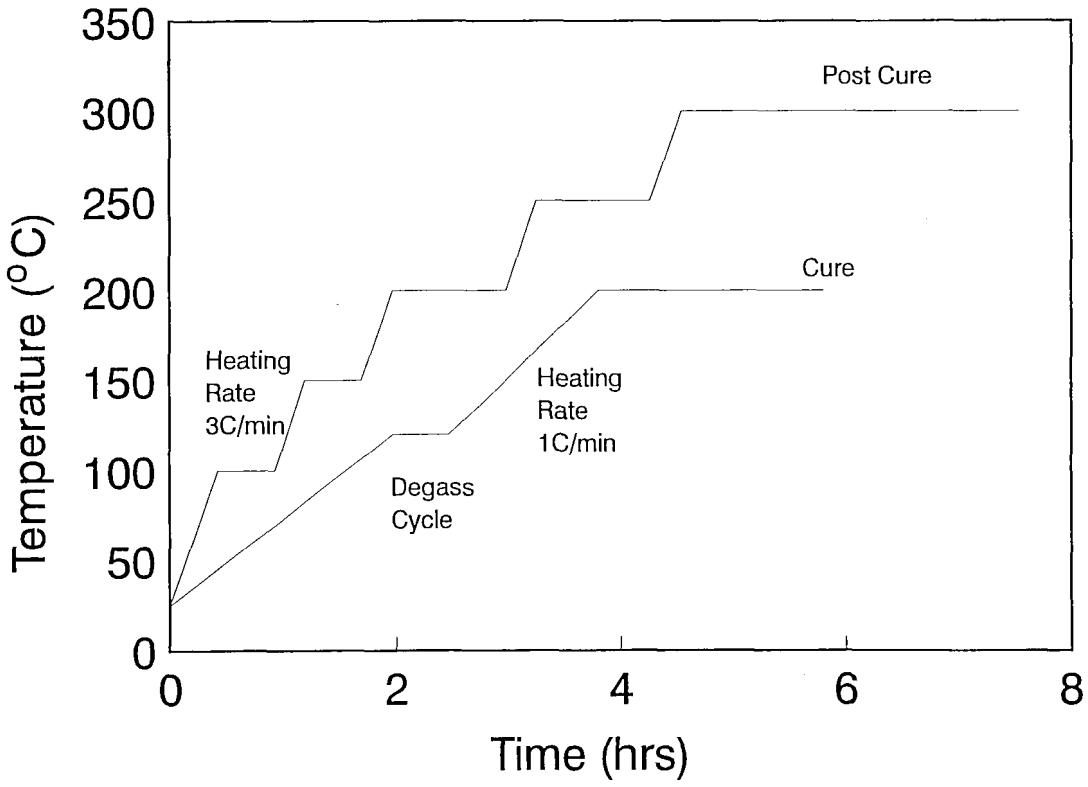

Figure 10. Cure and post cure cycles for the PT resin and the PT/TPI blends.

seen in the diagram in Figure 10. Specimens for each of the tests were machined for the post cured plaques to the dimensions given below. The unmodified plaques were too brittle after post cure and cracked during machining. These specimens were machined after cure and then subsequently post cured as described above.

2.4 DYNAMIC MECHANICAL PROPERTIES

Dynamic mechanical properties were determined with a Rheometrics RDAII controlled by a dedicated IBM computer work station. Specimens were tested in a torsional oscillating mode with a constant strain amplitude of 0.1% and a fixed frequency of 10 radians/second. Rectangular bar specimens measuring 50 mm X 12.5 mm X 2.5 mm were tested over a temperature range from 50°C to 450°C at 5°C/minute. Glass transition temperatures and phase separation were determined from the G' and tan delta thermal curves. Reported results are for one run per formulation.

2.5 COMPRESSIVE YIELD STRENGTH

Compression test were performed on polymer specimens (5.08 mm X 5.08 mm X 10.16 mm) according to ASTM D695 guidelines. Specimens were deformed in uniaxial compression in an Instron test machine run at a crosshead rate of .5 mm/minute. Yield strengths were determined from the intercepts of the tangents before and after the first break

in the stress strain curve (see for example Lee [43]). Reported results are an average of five tests per material. Tests were performed at 23°C.

2.6 FLEXURAL MODULUS

Flexural modulus measurements were made using a three-point bend test per ASTM D790. Specimens for flexural testing were unnotched rectangular bars measuring 63.5 mm X 12.5 mm X 1.6 mm. A support span of 50.8 mm (corresponding to a span to thickness ratio of 32/1) was used to reduce the shear component to the modulus value. Tests were performed at a rate of 2.45 mm per minute. All tests were conducted at 23°C. Flexural modulus values were calculated based on the following equation:

$$E = L^3m/4bd^3 \qquad (8)$$

where: E = flexural modulus of elasticity
L = support span
b = specimen width
d = specimen depth
m = slope of the tangent to the initial straight-line portion of the load defection curve

Reported results are the average of three specimens per formulation.

2.7 FRACTURE TOUGHNESS

Values of fracture toughness (K_{Ic}) were obtained by measuring the onset of unstable crack propagation in compact tension (CT) specimens. Because of the large amount of material required compared to the amount of material available, as well as the highly exothermic nature of the PT resin, particularly when curing large plaques, typical ASTM E399 specimens were not used. A NASA-developed miniaturized compact tension geometry (12.7 mm X 12.7 mm X 5.08 mm) was employed. Similar size specimens have been used previously and acceptable results were obtained [44,45]. Reported results are an average of five load excursions per formulation.

The compact tension specimens were precrack in the following manner. The specimens were first notched with a fine serrated Exacto blade. A razor blade which was kept in liquid nitrogen was then inserted into the notch and lightly tapped with a small hammer. A fresh razor blade edge was for each specimen. A high intensity focused light source was used to insure that the crack had propagated well away from the notch. This method of precracking consistently provided sharp cracks.

The unmodified PT resin samples were too brittle for the above procedure. All attempts to introduce a crack were unsuccessful and the final result was complete cleavage of

the specimens. For these samples, an alternative procedure for preparing the crack was used. The specimens were preheated to 300°C for 10 minutes. While the specimen was still hot, a razor was then inserted into the notch and slight pressure was applied. This produces a sharp straight crack extending well away from the notch.

To determine the fracture toughness, the precracked compact tension specimens were placed in a servohydralic MTS machine and tested in displacement control at a rate on 0.051 mm/min. By unloading the specimen immediately after fracture occurred and subsequently reloading it, multiple fractures were obtained from each specimen for tougher blends. The load versus displacement curves were recorded for each fracture.

The fracture toughness values were calculated based on the following equation:

$$K_{Ic} = (P/BW^{1/2}) * f(a/W) \qquad (9)$$

where: P is the critical load for crack propagation
B is the thickness
W is the specimen width
a is the crack length
and f(a/W) is the non-dimensional shape factor given by

$$f(a/W) = (2+a/W)\,(0.866 + 4.64a/W - 13.32a^2/W^2 + 14.72a^3/W^3 - 5.6a^4/W^4)/(1 - a/W)^{3/2} \qquad (10)$$

Due to the sample geometry of the mini-compact tension specimens, it was assumed that plane strain conditions were met. The validity of this assumption regarding the K measurement was evaluated using the ASTM E399 standard equation which determines whether the thickness is large enough to provide plane strain constraint: $t > 2.5\ (K_{Ic}/\sigma_y)^2$. Calculations for satisfying the plane strain constraint are discussed in the result section. All specimens in this work have the required dimensions for plane strain conditions.

2.8 SCANNING ELECTRON MICROSCOPY

Scanning electron microscopy was used to examine the fracture surfaces of the failed compact tension specimens. Examinations were performed using an AMR Model 100 scanning electron microscope. The accelerating voltage was 20kV. Samples were prepared by sputtering a thin layer of gold on the fracture surface to reduce any charge build-up.

Scanning electron microscopy was also used to the damage zones at the crack tip of unfailed compact tension specimens. Samples were prepared from precracked CT specimens. These specimens were loaded to 80 to 90 percent of the critical load for crack propagation then unloaded. The specimens were then wedged open and mounted in a room temperature curing epoxy. SEM samples were obtained by milling the mounted specimen to near the middle and then

polishing. The polished surface was then gold sputtered and examined by SEM.

3. RESULTS

3.1 DYNAMIC MECHANICAL ANALYSIS

Dynamic mechanical thermal curves for the unmodified resin, the thermoplastic modifier, and a blend containing 16% thermoplastic are shown in Figures 11 through 13. The glass transition temperatures for the unmodified resin and the modifier as shown are 417°C and 345°C respectively. The thermal curves for the resin/thermoplastic blend exhibits two distinct peaks. These peaks correspond well with the peaks for the two pure components. The Tg's for the blends studied vary between 336°C and 340°C for the thermoplastic component and 420°C and 426°C for the thermosetting resin. There however appears to be no significant or systematic change in the Tg of either component due to the blending. Due to the high Tg of the thermoplastic as seen by DMA, the use temperature of the toughened materials is maintained above 300°C.

Figure 14 shows a composite of the tan delta thermal curves for all the blends studied. As seen in this figure, the lower temperature peak, associated with the thermoplastic component, increases in magnitude with increasing amount of thermoplastic material. The higher

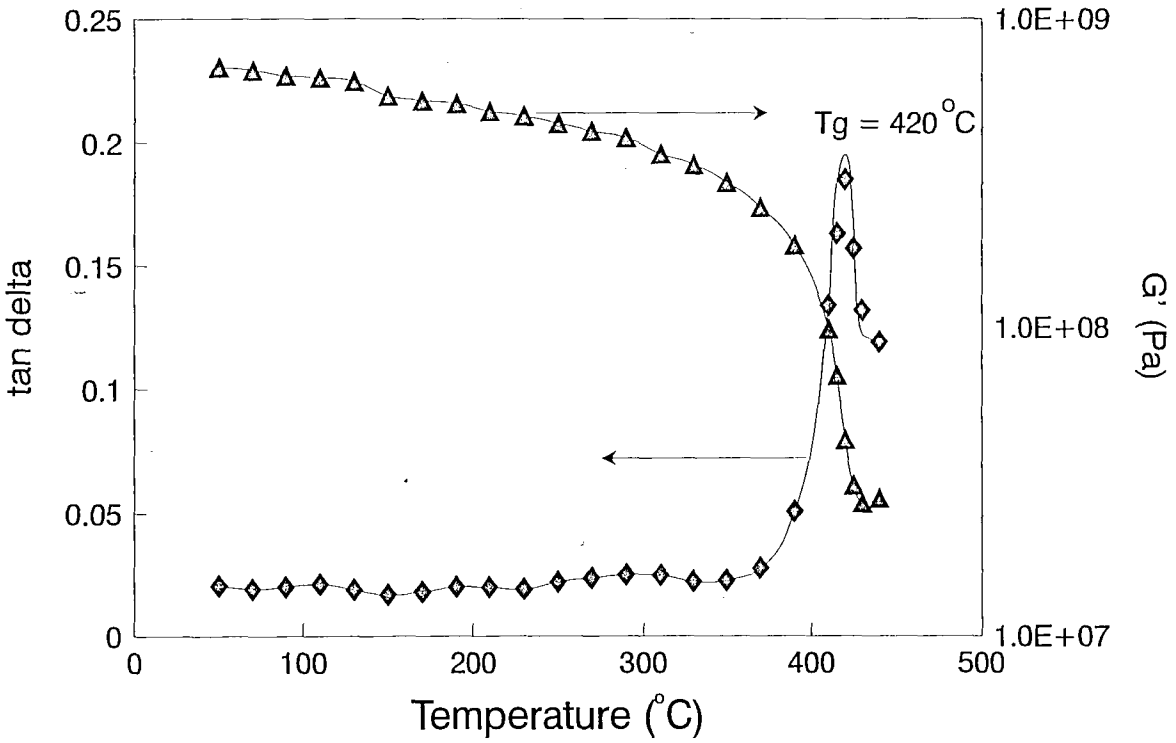

Figure 11. DMA thermal curve for unmodified PT resin.

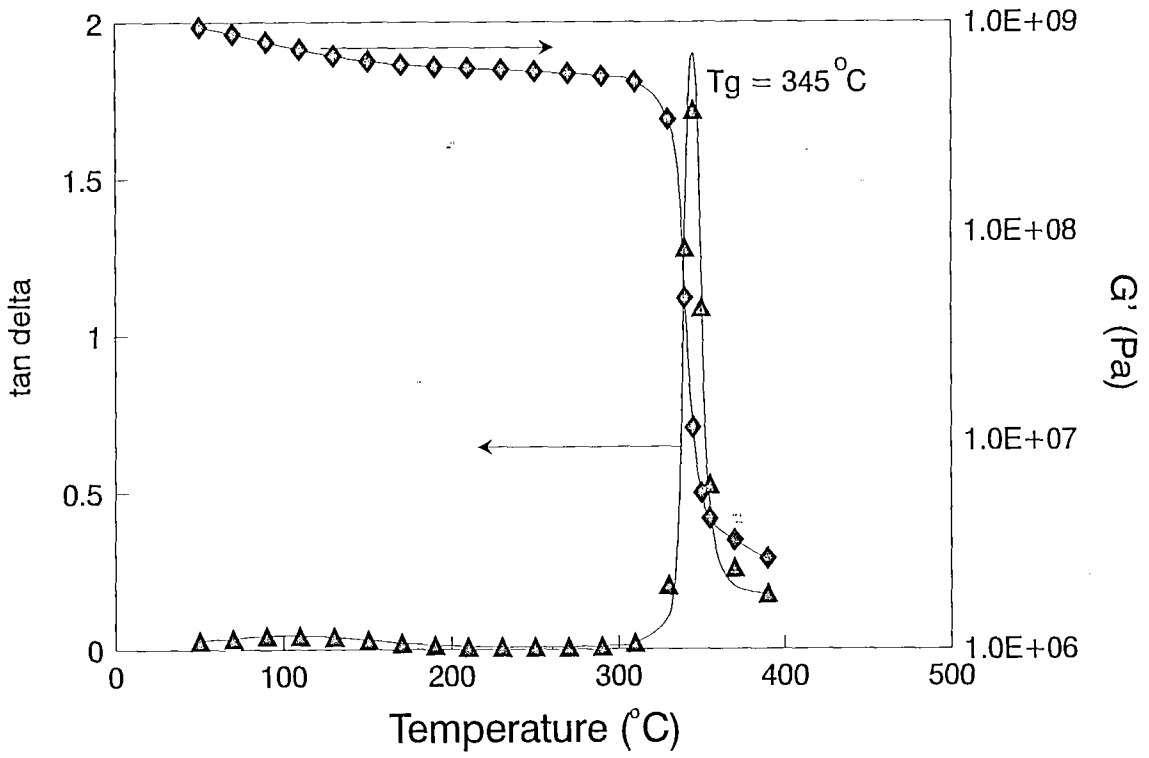

Figure 12. DMA thermal curve for TPI modified.

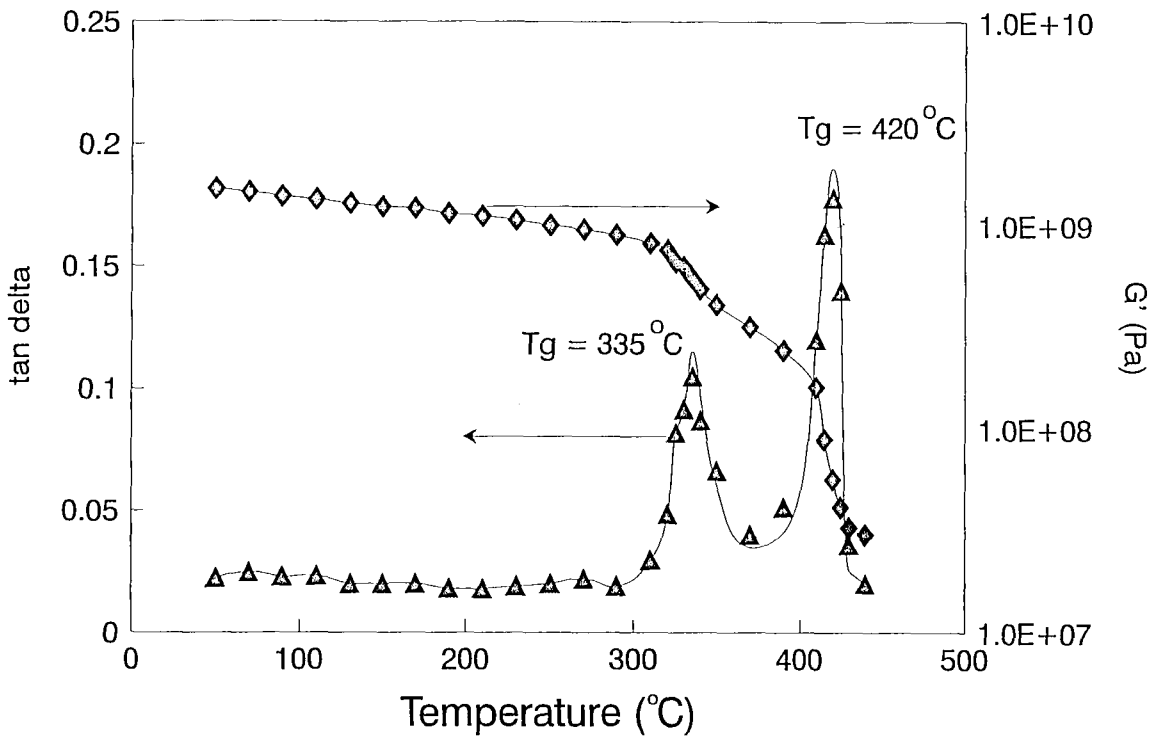

Figure 13. DMA thermal curve for blend containing 84% PT/16% TPI exhibiting a two phase morphology. The Tg of the two phases are equal to the pure components indicating no solubility between the phases.

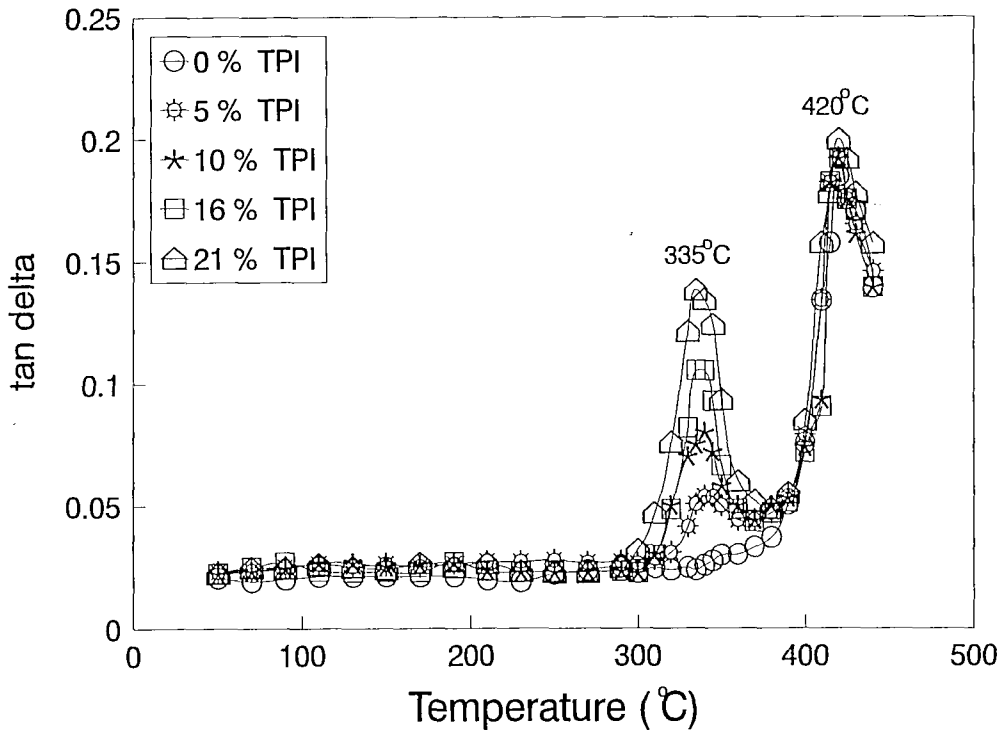

Figure 14. DMA thermal curve for PT/TPI blends again exhibiting a two phase morphology. The peak height of the thermoplastic Tg increase nearly proportionally with increasing volume fraction or TPI.

temperature peak remain relatively unchanged with respect to the amount of thermoplastic. The main feature of these plots is the high degree of phase separation that exists in the blends. The two phase nature of the blends is not surprising since the thermoplastic component was not soluble in the thermosetting resin. DMA thermal curves for all the formulations tested are shown in Appendix A.

3.2 COMPRESSIVE YIELD STRENGTH

The results of the compression testing are shown in Table II. As seen in this table, the unmodified resin displayed a yield strength of 214 MPa and the blend containing 21 percent modifier displayed a yield strength of 190 MPa. This corresponds to a decrease in 11%. A plot of the yield strength versus volume fraction of thermoplastic is shown in Figure 15. As seen in this plot there is some degree of scatter in the data but the plot gives a reasonably good fit to a linear plot. In general, only a slight decrease in compressive yield due to the addition of the thermoplastic component was observed.

3.3 FLEXURAL MODULUS

The flexural moduli were measured for the unmodified resin, the 84%PT/16%TPI blend, and the pure thermoplastic materials. The flexural moduli for these materials are 4.06 GPa, 3.89 GPa, and 3.10 GPa respectively. These data show

only a 4% decrease in modulus for the blend containing 16% modifier. This is as to be expected due to the relatively small difference in moduli (25%) between the resin and modifier. Based on the measured modulus data, modulus values for the other blends can be predicted by linear regression as seen in Figure 16.

3.4 FRACTURE TOUGHNESS

As mention previously, the fracture toughness measurements were made using a miniaturized CT test. Due to the small size of these specimens, only three crack length measurements were made, one at each edge of the specimen and one in the middle of the specimen. The overall crack length was calculated as a average of these three measurements.

Previous work by Lee and Jones [44] showed that the crack front for the miniaturized CT specimens exhibited a high degree of curvature, and thus a weighted average crack length measurement was used. The crack fronts exhibited by the specimens in this work did not show the same degree of curvature and a straight averaged crack measurement was used. Appendix B gives the results of the CT tests and summarized in Table II. As seen in this data there is some degree of scatter within the samples but this is relatively small for this type of test.

Table II

Mechanical Properties of PT/TPI Blends

V_f	σ_{yc} (MPa)	E (GPa)	K_{Ic} (MPa $m^{1/2}$)	G_{Ic} (J/m^2)
0	214	4.05	0.430	38.4
5	216	4.00	0.509	54.4
10	200	3.96	0.545	63.0
16	206	3.90	0.602	78.1
21	190	3.85	0.659	94.7

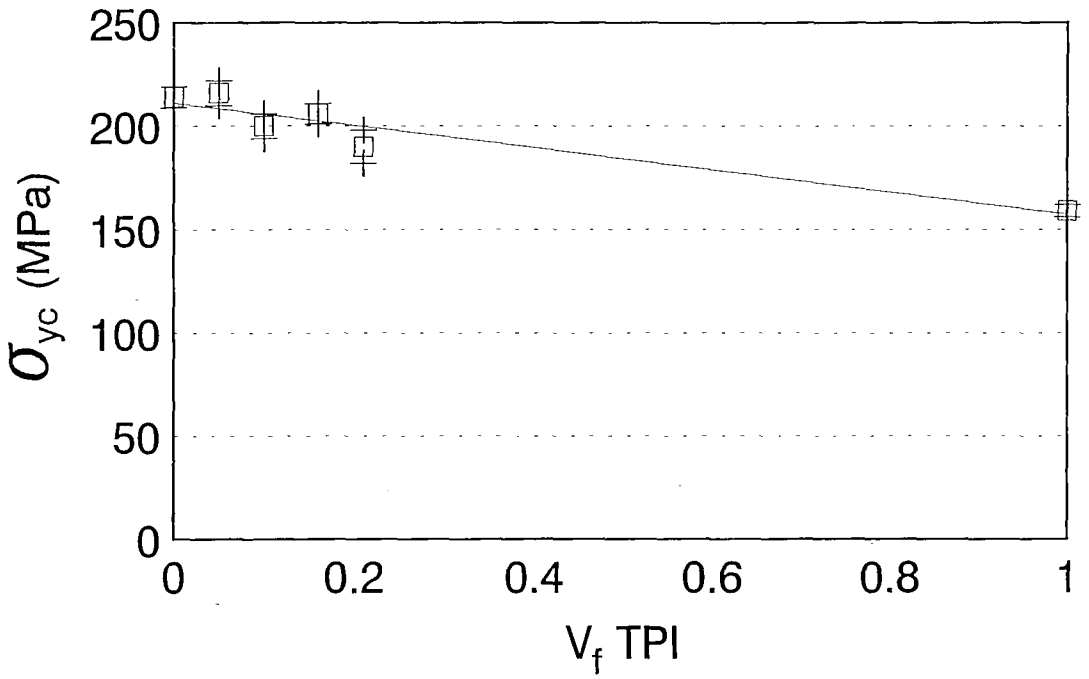

Figure 15. Compressive yield strength versus volume fraction of TPI. There is no significant decrease in compressive yield strenght due to the addition of the thermoplastic modifier. The linear decrease in σ_{yc} generally follows the rule of mixtures.

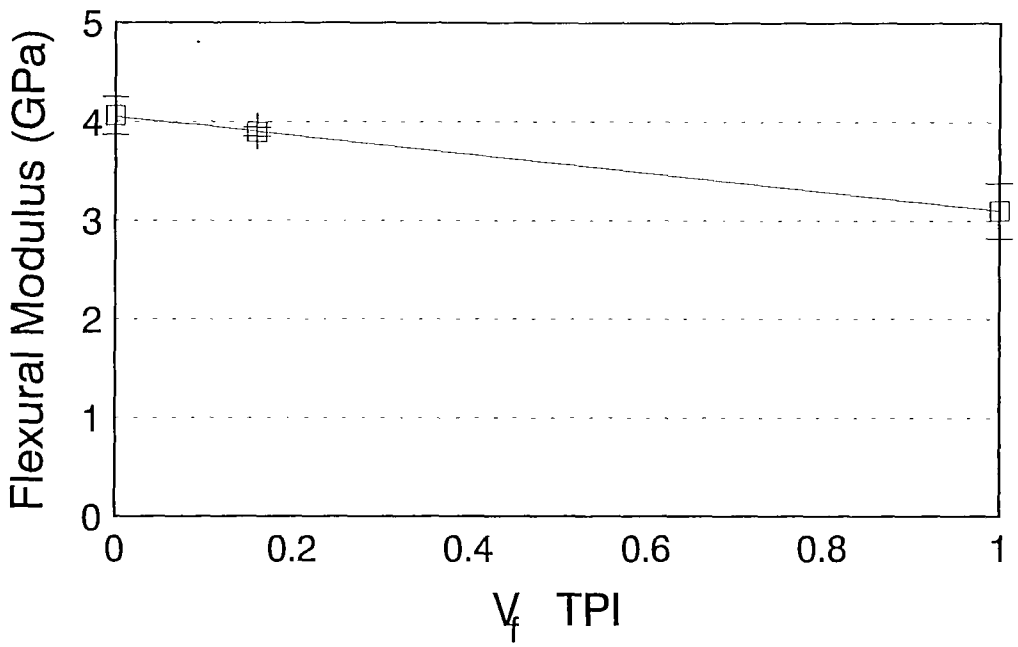

Figure 16. Flexural modulus versus volume fraction of TPI. There is no significant decrease in flexural modulus due to the addition of the thermoplastic modifier. The linear decrease in E generally follows the rule of mixtures.

The validity of the K_{Ic} measurement was evaluated using the ASTM E399 standard equation. Since these polymers did not exhibit tensile yield, the constraint was solved for yield stress using the measured Kq values. Sample calculation are shown in Appendix C. In order for plane strain conditions to not be met, these samples would have to posses a tensile yield stress less than 12.6 MPa corresponding to 10% of the measured compression yield stress. This is very unlikely and thus the specimens have the requisite dimensions for plane strain conditions.

The fracture toughness, K_{Ic} of the TPI modified PT resin increases nearly linearly with TPI content. A plot of the fracture toughness versus TPI volume fraction is shown in Figure 17. As seen from this figure, the magnitude of the increase in toughness in modest, ΔK_{Ic} = 0.23 MPa $m^{1/2}$, it corresponds to a 50% increase in toughness over the unmodified resin.

3.5 SCANNING ELECTRON MICROSCOPY

Scanning electron microscopy was performed on the fracture surfaces of tested compact tension specimens. Micrographs for the 5, 10, 16, and 21% loaded resin blends are shown in Figures 18 - 21 respectively. Examination of the micrographs clearly indicates that there is no evidence of particle pull-out indicating good adhesion between the resin and the thermoplastic modifier.

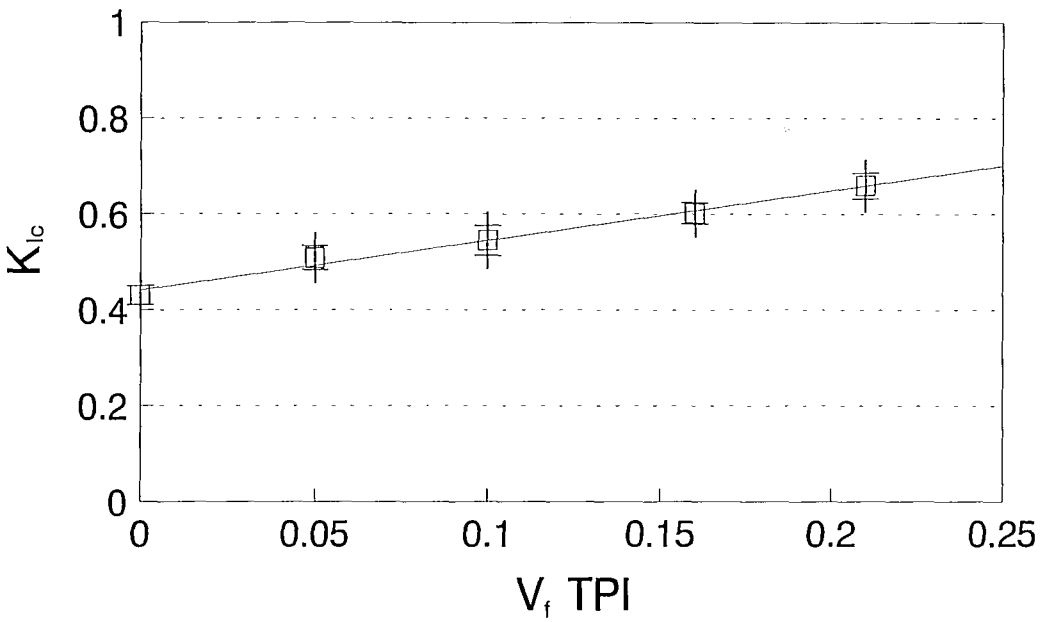

Figure 17. Fracture toughness K_{Ic} versus volume fraction of TPI. The toughness increases linearly with increasing volume fraction.

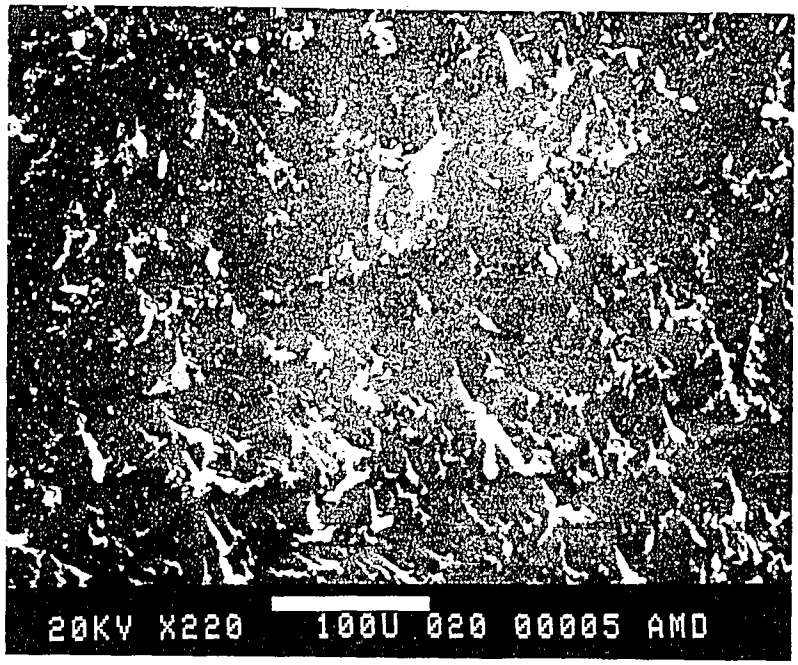

a) X220

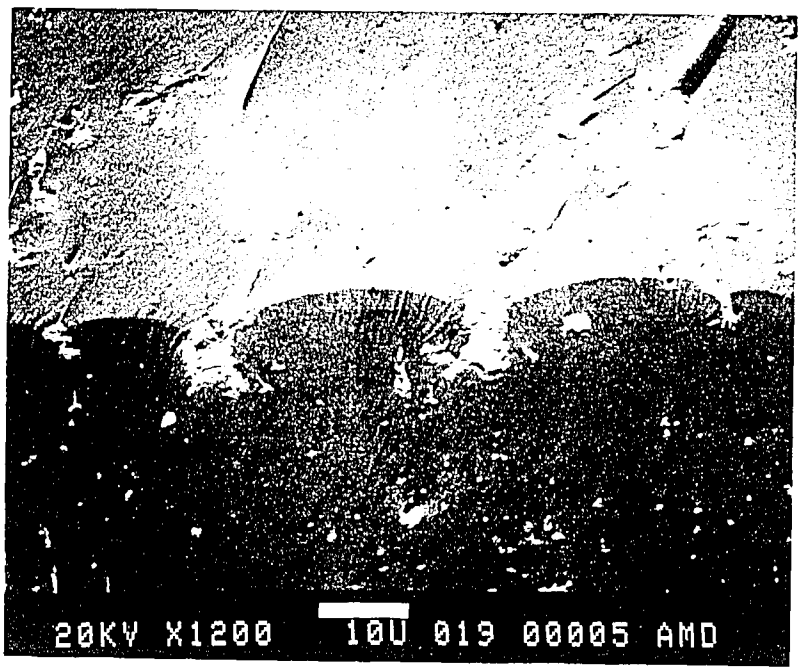

b) X1200

Figure 18. SEM micrographs of fracture surface for CT sample containing 95% PT/5% TPI. Note a) the very flat fracture surface and b) the presence of ductile tearing of the particle and bowing of the crack front between the particles.

a) X220

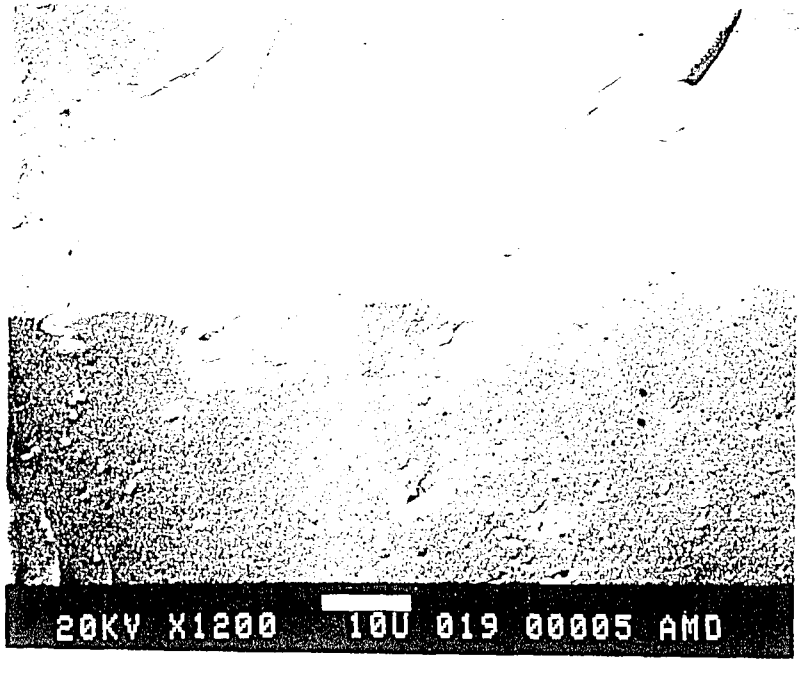

b) X1200

Figure 18. SEM micrographs of fracture surface for CT sample containing 05% PT/5% TPL. Note a) the very flat fracture surface and b) the presence of ductile tearing of the particle and bowing of the crack front between the particles.

a) X220

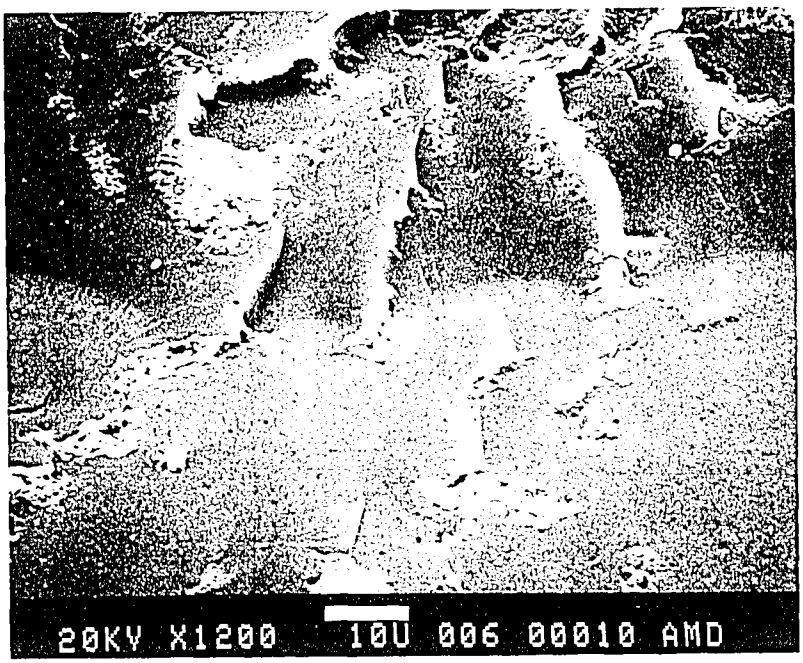

b) X1200

Figure 19. SEM micrographs of fracture surface for CT sample containing 90% PT/10% TPI. Note a) the relatively flat fracture surface and b) crack pinning is evident from the presence of bowing of the crack front and the "tails" behind the particles.

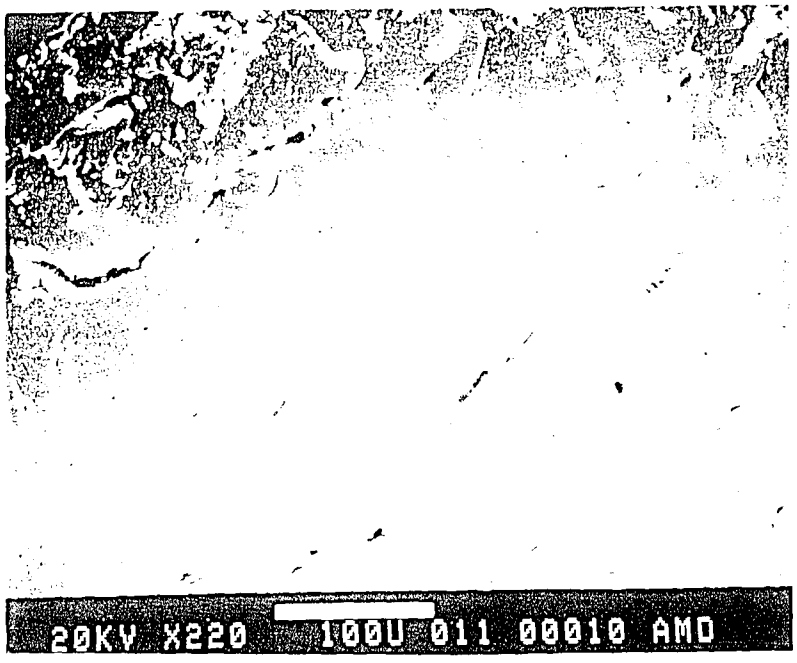

a) X220

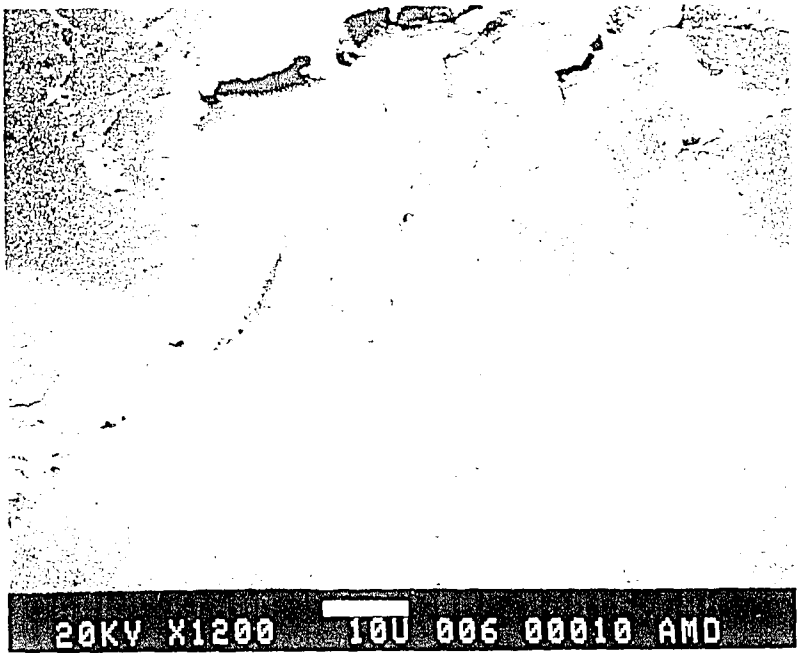

b) X1200

Figure 19. SEM micrographs of fracture surface for CI sample containing 90% PT 10% TPI. Note a) the relatively flat fracture surface and b) crack pinning is evident from the presence of bowing of the crack front and the "tails" behind the particles.

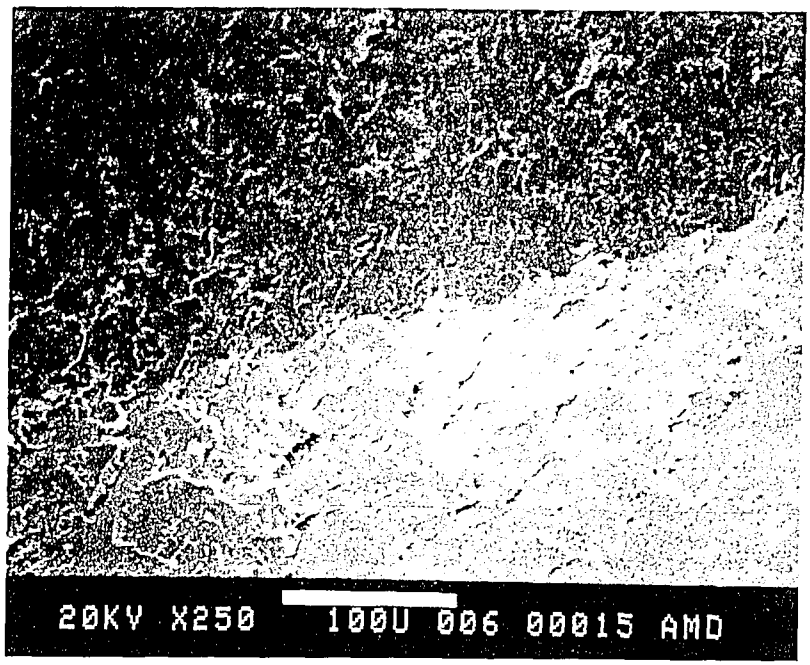

a) X250

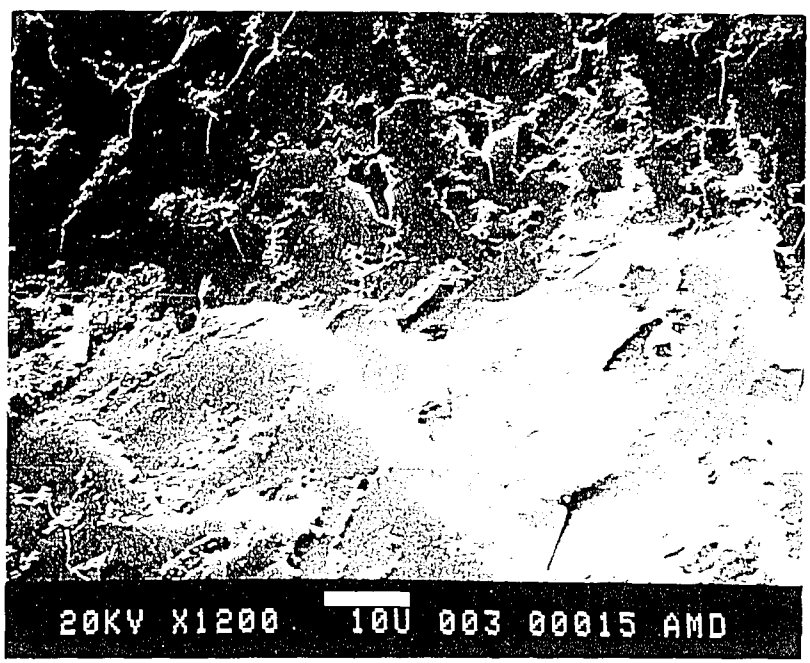

b) X1200

Figure 20. SEM micrographs of fracture surface for CT sample containing 84% PT/16% TPI. Note a) the fracture surface has become very rough and b) crack pinning is still evident along with many fracture steps indicating possible interaction will particles above and below the crack plane.

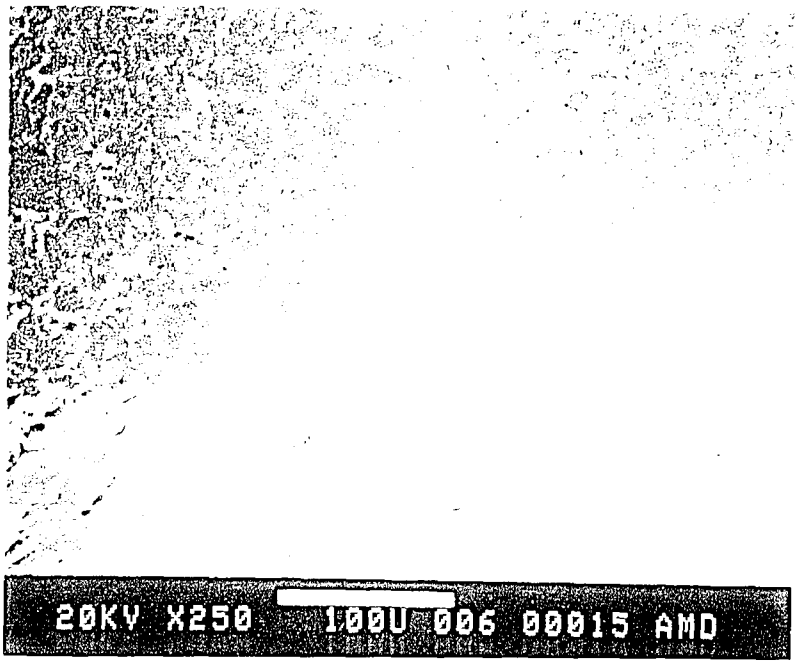

a) X250

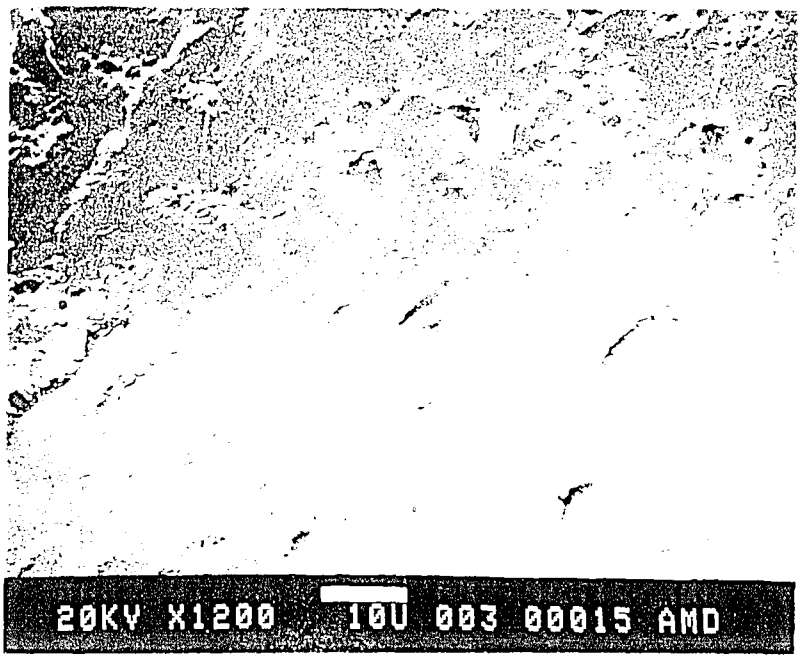

b) X1200

Figure 26. SEM micrographs of fracture surface for CT sample containing 84% PI 168 TPI. Note a) the fracture surface has become very rough and b) crack pinning is still evident along with many fracture steps indicating possible interaction will particles above and below the crack plane.

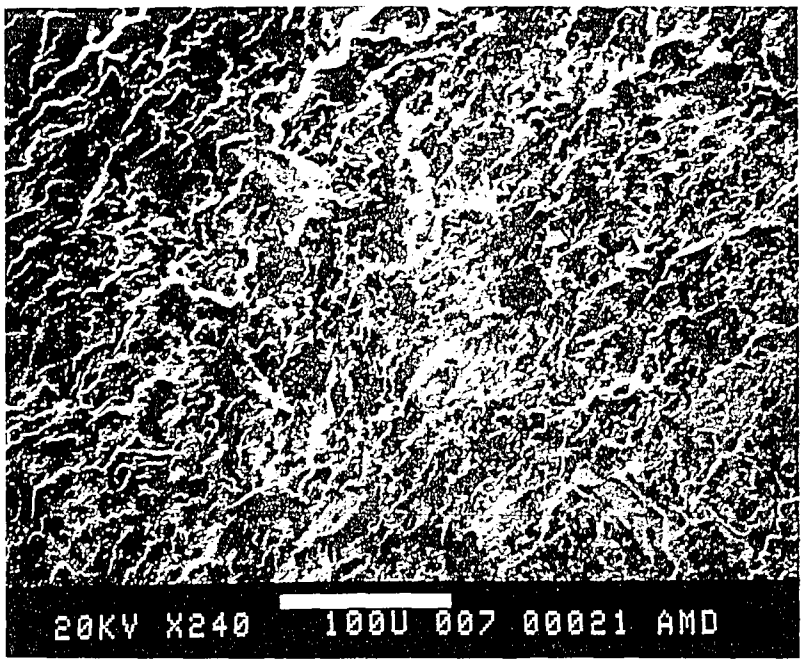

a) X240

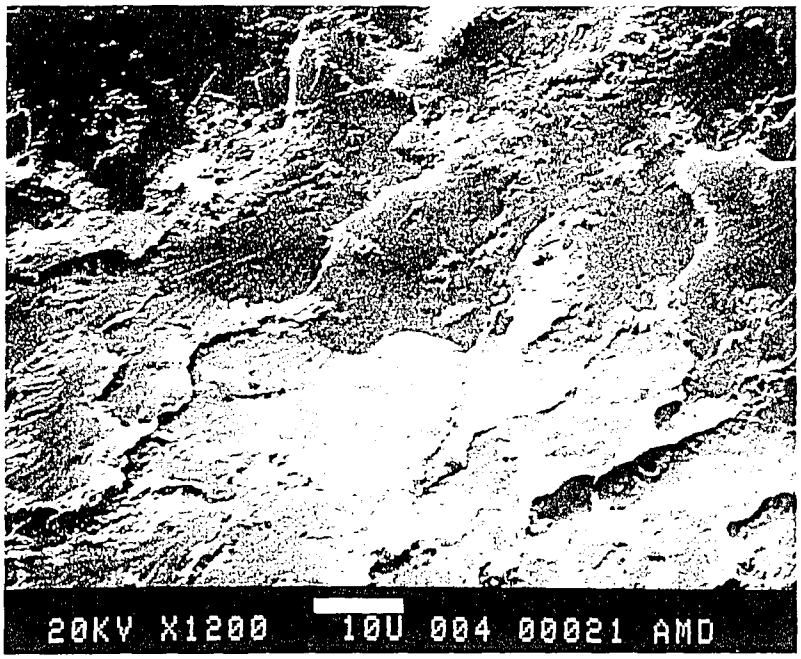

b) X1200

Figure 21. SEM micrographs of fracture surface for CT sample containing 79% PT/21% TPI. Note a) the fracture surface has become very rough and b) crack pinning and ductile tearing of the particles along with many fracture steps indicating possible interaction will particles above and below the crack plane.

a) X240

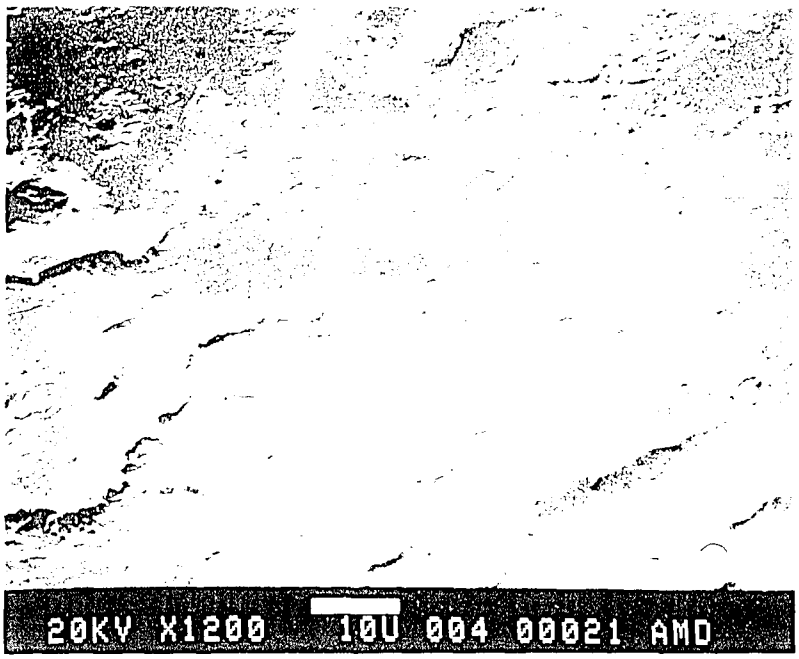

b) X1200

Figure 21. SEM micrographs of fracture surface for C1 sample containing 79% PT-21% TFI. Note a) the fracture surface has become very rough and b) crack pinning and ductile tearing of the particles along with many fracture steps indicating possible interaction will particles above and below the crack plane.

The source of toughness improvements can be determined by examining the SEM micrographs. These micrographs present evidence of particle tearing in all modified blends. Closer examination reveals that for the lower thermoplastic loading levels, the fracture surface is very flat even under high magnification (Figure 18b). At higher loading levels, the scanning electron micrograph reveals many fracture steps in the surface of the CT specimen as seen in Figure 21b for the PT resin with 21% TPI. In addition to particle tearing, there is evidence of crack pinning. This is displayed in Figure 19b as noted by the "tails" behind the particles and crack bowing between two thermoplastic particles. This evidence is very similar the that presented by Kinloch et al. [27] for glass spheres in a glass-filled epoxy.

SEM micrographs of the damage zone at the crack tip were examined to determine the presence of microcracking. Figure 22 shows a through-thickness micrograph of a PT/TPI blend containing 16% thermoplastic. As seen in Figure 22, there is no evidence of microcracking at the crack tip as was reported by Pearson [16] for PPO modified epoxy systems.

4. DISCUSSION

4.1 TOUGHENING MECHANISMS

Several toughening mechanisms have been proposed to explain the increase in toughness associated with the

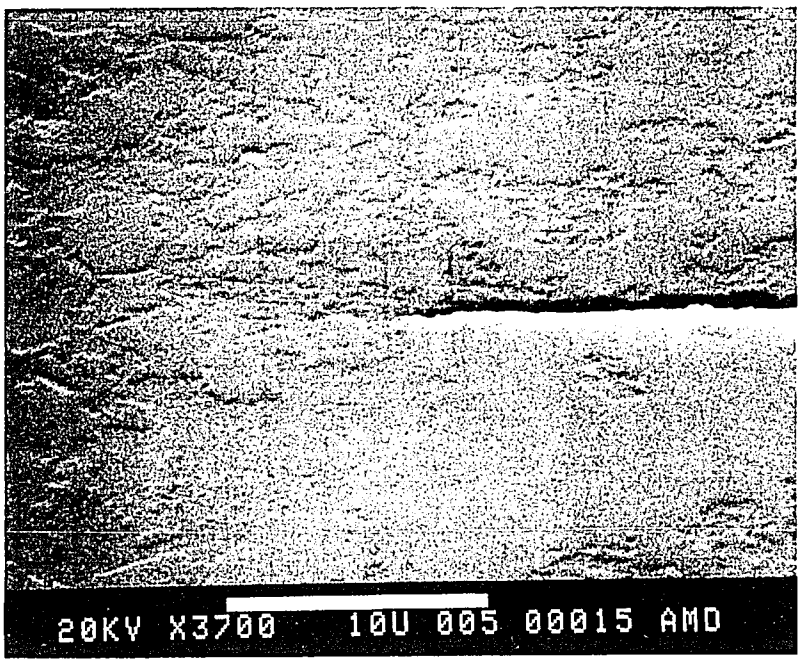

Figure 22. SEM micrograph of the crack front in a CT specimen view through the thickness. There is no evidence of microcracking occurring ahead of the crack tip.

addition of thermoplastic modifiers to a thermosetting resin. Of these mechanisms, there is evidence of crack bridging and crack pinning in the polymer system studied. In order to assess the contribution of these mechanisms to the overall increase in toughness model for each of these mechanisms will be examined. Ashby et. al. [46] developed a model to account for the increase in toughness for ductile particles that bridge the crack in a brittle matrix as a function of the properties and adhesion of the included particles. Bridging particles will increase the toughness if the particles span the advancing crack and stretch as the crack opens until the particles fracture or decohere. The work of stretching contributes to the overall toughness of the material. The amount of stretching is dependent on the adhesion between the particle and the matrix.

$$K_{Ic}' = K_{Ic}^{o} + E \left[C V_f \sigma / E a_o \right]^{1/2} \quad (11)$$

where K_{Ic}' is the fracture toughness of the modified resin
K_{Ic}^{o} is the fracture toughness of the unmodified resin
E is the modulus of the thermoplastic modifier
σ is the yield stress of the thermoplastic modifier
V_f is the volume fraction of thermoplastic
a_o is the radius of the thermoplastic particles
C is constant relating the extent of adhesion between the particle and the matrix.

Ashby reports that values for *C* can range from 1.6 for complete bonding to 6 for limited debonding . As seen by this model, limited debonding of the particle and matrix

provides more toughness than complete bonding. If the particle is strongly bonded, it will be constrained and the amount of stretching that the particle can undergo prior to failure will be significantly reduced. Limited particle/matrix debonding will allow for more stretching of the particle prior to particle fracture. This amount of stretching the particle undergoes is important because the energy absorbed during stretching in crucial in the overall contribution to the toughness.

The expected increase in toughness based on a crack bridging mechanism can be determined by using Ashby's model. The properties of the toughener were based on thin film data supplied by the manufacturer [41]. Thin film data was used instead of bulk properties in an attempt to more accurately represent the properties of the particle. The modulus and yield stress of the thermoplastic modifier were 2.9 GPa and 85.5 MPa receptively. The particle radius was taken to be between 2.5 and 5 μm and a value of 1.6 was be used as the adhesion factor due to the good particle/matrix adhesion as seen in the SEM micrographs. The increase in fracture energy as a function of V_f can be seen in Figure 23.

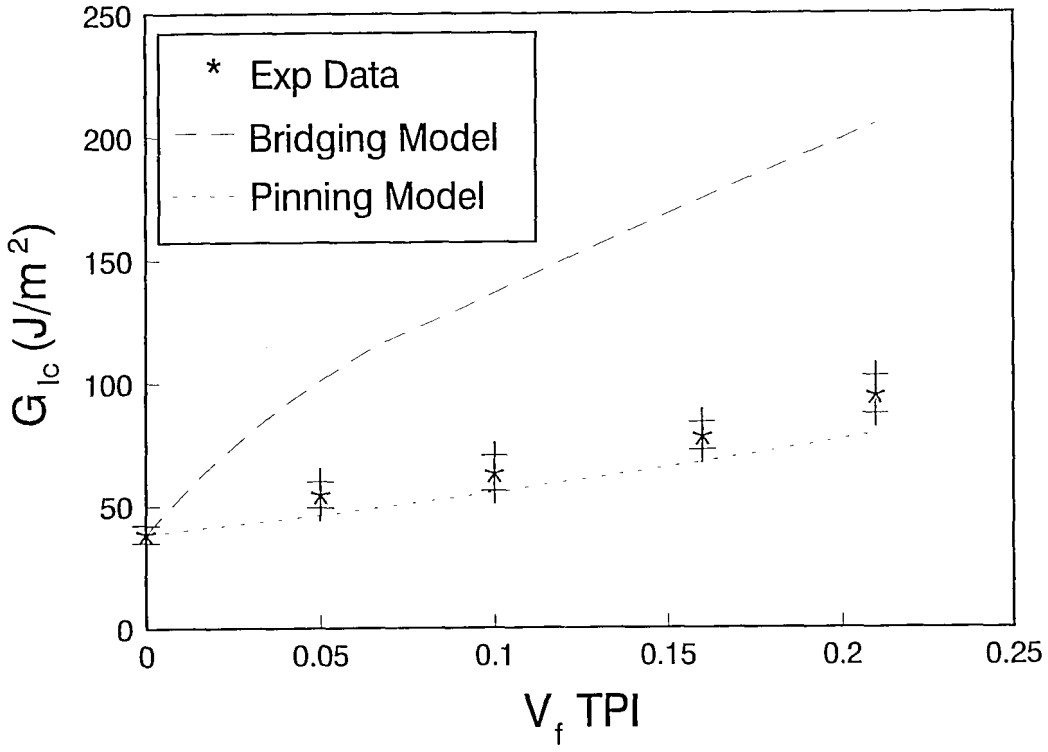

Figure 23. Fracture energy G_{Ic} versus volume fraction of TPI comparing experimental data, the crack bridging model and the crack pinning model. The crack pinning model more accurately correlates with the increase in toughness measured experimentally indicating that the dominant toughening mechanism is crack pinning.

The crack pinning models have been discussed in the introduction, of these models, the one proposed by Lange [28] provides for a linear increase in fracture energy with increasing volume fraction of filler. As mentioned previously, Lange's model is:

$$G_{Ic}' = G_{Ic}^{o} + 2T/d_s \qquad (3)$$

where G_{Ic}' is the fracture energy of the modified resin.
G_{Ic}^{o} is the fracture energy of the unmodified resin.
T is the line tension.
d_s is the center-to-center particle spacing.

An expression for the line energy of the crack front can given by the following equation:

$$T = G_{Ic}^{o}/3 * \mathbf{c} \qquad (12)$$

where **c** is defined as the radius of the circular crack.

Using an equation to approximate the center-to-center particle spacing:

$$d_s = (2d_p * (1 - V_f))/3V_f \qquad (13)$$

where d_p is the particle diameter [30] the overall equation for increase in fracture energy becomes:

$$G_{Ic}' = G_{Ic}^{o} + (G_{Ic}^{o} * \mathbf{c})/d_p*(V_f/(1-V_f)) \qquad (15)$$

c can be determined by calculating the radius of the crack front in Appendix D. Using an average radius of between 25

and 30 μm and an average particle size of between 5 and 10 μm, the calculated increase in fracture energy versus V_f can be seen in Figure 23 along with the experimental data.

As seen by Figure 23, the crack bridging model over predicts the toughness increase while the crack pinning model correlates well the experimental data. The over prediction of the toughness by the crack bridging model maybe due the good adhesion of the TPI particles to the PT resin. This adhesion constrained the particle causing failure of the TPI particle before they could span the crack. The crack pinning model gives a reasonable fit to the experimental data presented here. Thus it is unlikely that the crack bridging mechanism significantly contributed to the increase in toughness and the increase in toughness is due predominantly to crack pinning. The good correlation of the experimental data may be somewhat fortuitous in light of the assumptions made in the application of the two models. In order to simplify the calculations, it was assumed that the TPI particles were spheres of constant diameter. It was also assumed that the plastic deformation energy γ_p is negligible compared to the surface energy γ_s. Qualitatively, the models appear to be an appropriate starting point for TPI modified PT resins investigated in this work. The material parameters used to generated the curves in Figure 23 appear to be reasonable.

4. CONCLUSIONS

Based on the results of these experiments and the evaluation of the two mechanistic models, the following conclusions can be made:

1. The addition of the TPI to the PT resin did not significantly reduce the Tg of the system and the temperature capability was maintained above 300°C.
2. The addition of the TPI to the PT resin did not adversely affect the flexural and compressive properties of the polymer for loadings up to 21% TPI by volume.
3. Addition of the TPI increase the fracture toughness of the PT resin by over 50% for a volume fraction of 21%.
4. The mechanism responsible for the increase in toughness is crack pinning, while there was some evidence of ductile tearing of the TPI particles, crack bridging did not significantly contribute to the overall increase in toughness.

6. FUTURE WORK

Further work is needed to isolate and investigate the parameters associated with each of the toughening mechanisms identified for the PT resin modified with TPI. The crack bridging model discussed previously identified the strength/stiffness of the particles and the particle to matrix adhesions as factors controlling the toughness. By varying the molecular weight or the chemical structure of a thermoplastic modifier, the effect of the particle strength/stiffness on toughness can be determined. The particle to matrix adhesion can be altered by the use of reactive endgroups or less compatible thermoplastic materials.

The crack pinning model related toughness to the particle size and spacing, as well as the line tension (the line tension is a function of the toughness of the unmodified resin). Addition research into this model should take a more rigorous approach to these parameters. The use of glass spheres as particles will provide a more uniform particle size and spacing. Measuring the toughness for a given particle size a several loading levels and for a range of particle sizes at one loading level should provide a more clear relation between toughness due to pinning and particle size. In addition, it would also be beneficial to investigate the effect of resin toughness on the crack pinning model. Donnellan et.al. [47] showed that the

toughness of an unmodified BMI resin can be controlled by changing the cure state. This approach can be applied to the PT resin, for a given particle size and loading, the cure cycle of the PT resin can be altered thus changing the toughness of the resin and ultimately the line tension of the system.

These further studies would be useful in developing a more in-depth understanding of the crack bridging and crack pinning mechanisms. In addition, the ability to toughen high temperature polymers through the use of second phase modifiers would be improved.

7. REFERENCES

1. A.F. Yee and R.A. Pearson, *J. Mat. Sci.*, 21 (1986) 2462.

2. R.A. Pearson and A.F. Yee, *J. Mat. Sci.*, 21 (1986) 2475.

3. A.J. Kinloch, S.J. Shaw, D.A. Tod and D.L. Hunston, *Polymer*, 24 (1983) 1341.

4. A.J. Kinloch, S.J. Shaw, and D.L. Hunston, *Polymer*, 24(1983) 1355.

5. R.A. Pearson and A.F. Yee, *J. Mat. Sci.*, 24 (1989) 2571.

6. A.J. Kinloch, S.J. Shaw, and D.A. Tod, Adv. Chem. Series 208 (1984) 101.

7. Y.P. Sachdeva, *Int. SAMPE Tech.*, 21 (1989) 1018.

8. C.B. Bucknall and I.K. Partridge, *Polymer*, 24 (1983) 639.

9. R.S. Raghava, *Int. SAMPE Symp.*, 28 (1983) 367.

10. J.L. Hedrick, I. Yilgor, G.L. Wilkes and J.E. McGrath, *Polym. Bull.*, 13 (1985) 201.

11. J.L. Hedrick, I. Yilgor, M. Jurek, J.C. Hedrick, G.L. Wilkes and J.E. McGrath, *Polmer*, 32 (1991) 2020.

12. J.A. Cecere and J.E. McGrath, *Polym. Preprts.*, 27 (1986) 299.

13. R.S. Raghava, *J. Polym. Sci.: Part B*, 26 (1988) 65.

14. Z. Fu and Y. Sun, *Polym. Preprts.*, 29 (1988) 177.

15. C.B. Bucknall and A.H. Gilbert, *Polymer*, 30 (1989) 213.

16. R.A. Pearson and A.F. Yee, *J. Appl. Poly. Sci.*, to be published (1993).

17. C.R. Lin, W.L. Liu, and J.T. Hu, *Int. SAMPE Symp.*, 34 (1989) 1803.

18. H.D. Stenzenberger, W. Romer, P.M. Hergeenrother, B. Jensen, and W. Breitigam, *Int. SAMPE Symp.*, 35 (1990) 2175.

19. S.P. Wilkinson, S.C. Liptak, P.A. Wood, J.E. McGrath, and T.C. Ward, *Int. SAMPE Symp.*, 36 (1991) 482.

20. N.J. Johnston, K. Srinivasan and R.H. Pater, *Int. SAMPE Symp.*, 37 (1992) 690.

21. Z.B. Ahmad, M.F. Ashby and P.W.R. Beaumont, *Scripta metall.*, 20 (1986) 843.

22. S. Kunz-Douglas, P.W.R. Beaumont, and M.F. Ashby, *J. Mat. Sci.*, 15 (1980) 1109.

23. S.C. Kunz and P.W.R. Beaumont, *J. Mat. Sci.*, 16 (1981) 2141.

24. R.A. Pearson and A.F. Yee, *J. Mat. Sci.*, 26 (1991) 3828.

25. L.R.F. Rose, *Mech Mater.*, 8 (1987) 11.

26. L.S. Sigl, P.A. Matage, B.J. Dalgleish, R.M. McMeeking, and A.G. Evans, *Acta metall.*, 36 (1988) 945.

27. A.J. Kinloch, D. Maxwell and R.J. Young, *J. Mat. Sci.Lett.*, 4 (1985) 1276.

28. F.F. Lange, *Phil Mag.*, 22 (1970) 983.

29. A.G. Evans, *Phil Mag.*,.26 (1972) 1327.

30. F.F. Lange and K.C. Radford, *J. Mat. Sci.*, 6 (1971) 1197.

31. D.J. Green, P.S. Nicholson, and J.D. Embury, *J. Mat. Sci.*, 14 (1979) 1657.

32. K.T. Faber and A.G. Evans, *Acta metall.*, 31 (1983) 565.

33. A.G. Evans and K.T. Faber, *J. Am. Cer. Soc.*, 67 (1983) 255.

34. J.W. Hutchinson, *Acta metall.*, 35 (1987) 1605.

35. M. Ortiz, *Trans. ASME*, 54 (1987) 54.

36. A.G. Evans and K.T. Faber, *J. Am. Cer. Soc.*, 64 (1981) 394.

37. A.G. Evans, S. Williams and P.W.R. Beaumont, *J. Mat Sci.*, 20 (1985) 3668.

38. F. Gao and T. Wang, *J. Mat. Sci Lett.*, 24 (1990) 1409.

39. S. Das, D.C. Prevorsek, and B.T. DeBona, *Int. SAMPE Conf.*, 21 (1989) 972.

40. S.A. Srinivasan, G.D. Lyle and J.E. McGrath, *Int. SAMPE Symp., 38* (1993) 28.

41. Polyimide XU218 Product Daa Sheet, Ciba Geigy, 1983.

42. Personal Communication with Dr. B.T. DeBona, Allied-Signal, May 1993.

43. W.H. Lee, K.A. Hodd and W.W. Wright, *J. Mat. Sci.*, 27 (1992) 4582.

44. C.Y-C Lee and W.A. Jones, *Polym. Eng. Sci.*, 22 (1982) 1190.

45. J.A. Hinkley, *J. Appl. Polym. Sci.*, 32 (1986) 5653.

46. M.F. Ashby, F.J. Blunt and M. Bannister, *Acta metall.*, 37 (1989) 1847.

47. T.M. Donnellan, P.A. Mehrkam, A. Yen, R. Jurek and R.J. Morgan, *ACS Tech. Conf.*, 6 (1991) 3.

Appendix A. DMA thermal curves for unmodified resins and PT/TPI blends.

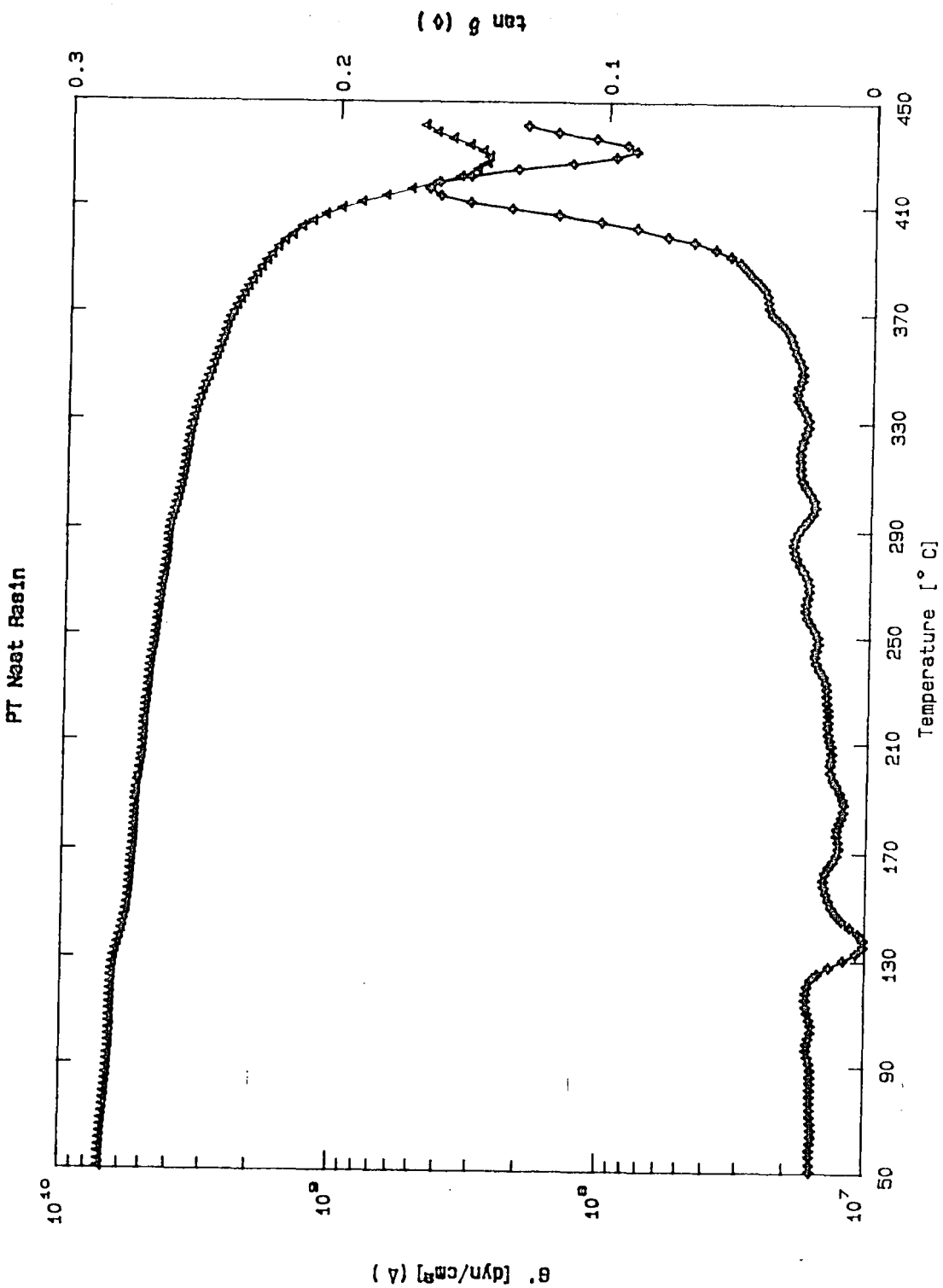

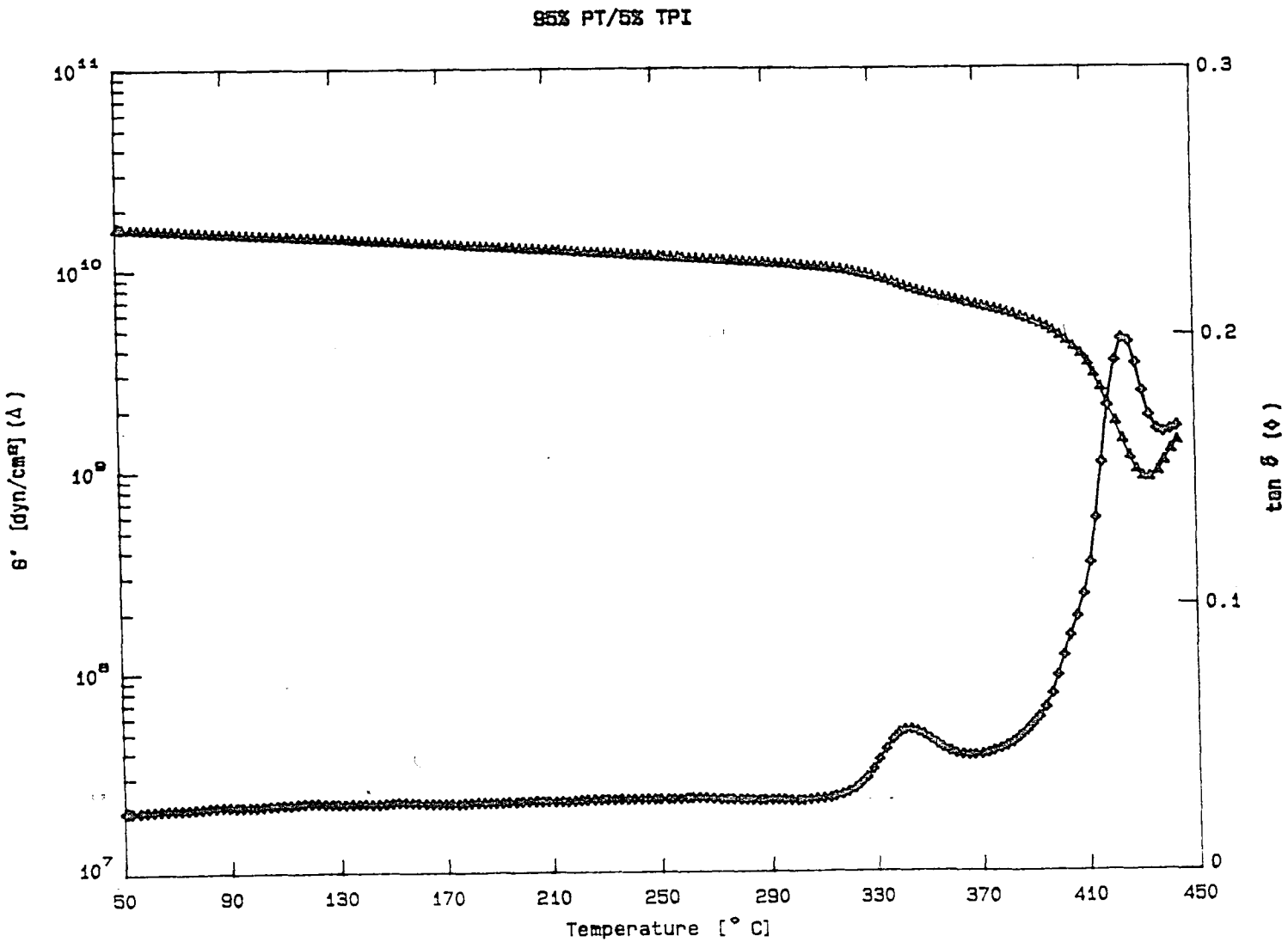
95% PT/5% TPI
10^{11}
10^{10}
10^{9}
10^{8}
10^{7}
G' [dyn/cm²] (Δ)
0.3
0.2
0.1
0
tan δ (◇)
50
90
130
170
210
250
290
330
370
410
450
Temperature [° C]

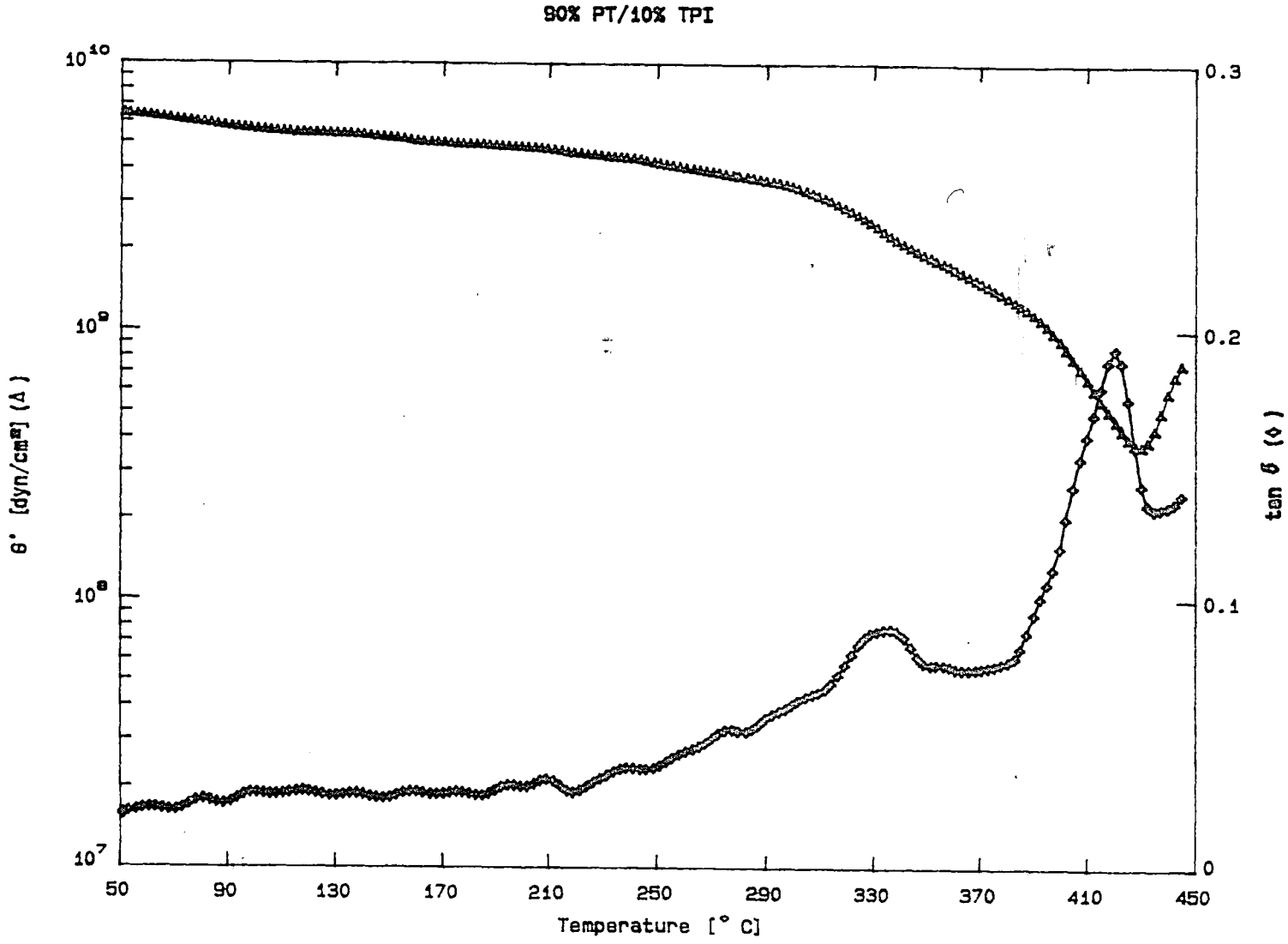
90% PT/10% TPI
10^{10}
10^{9}
10^{8}
10^{7}
G' [dyn/cm²] (Δ)
0.3
0.2
0.1
0
tan δ (◇)
50
90
130
170
210
250
290
330
370
410
450
Temperature [° C]

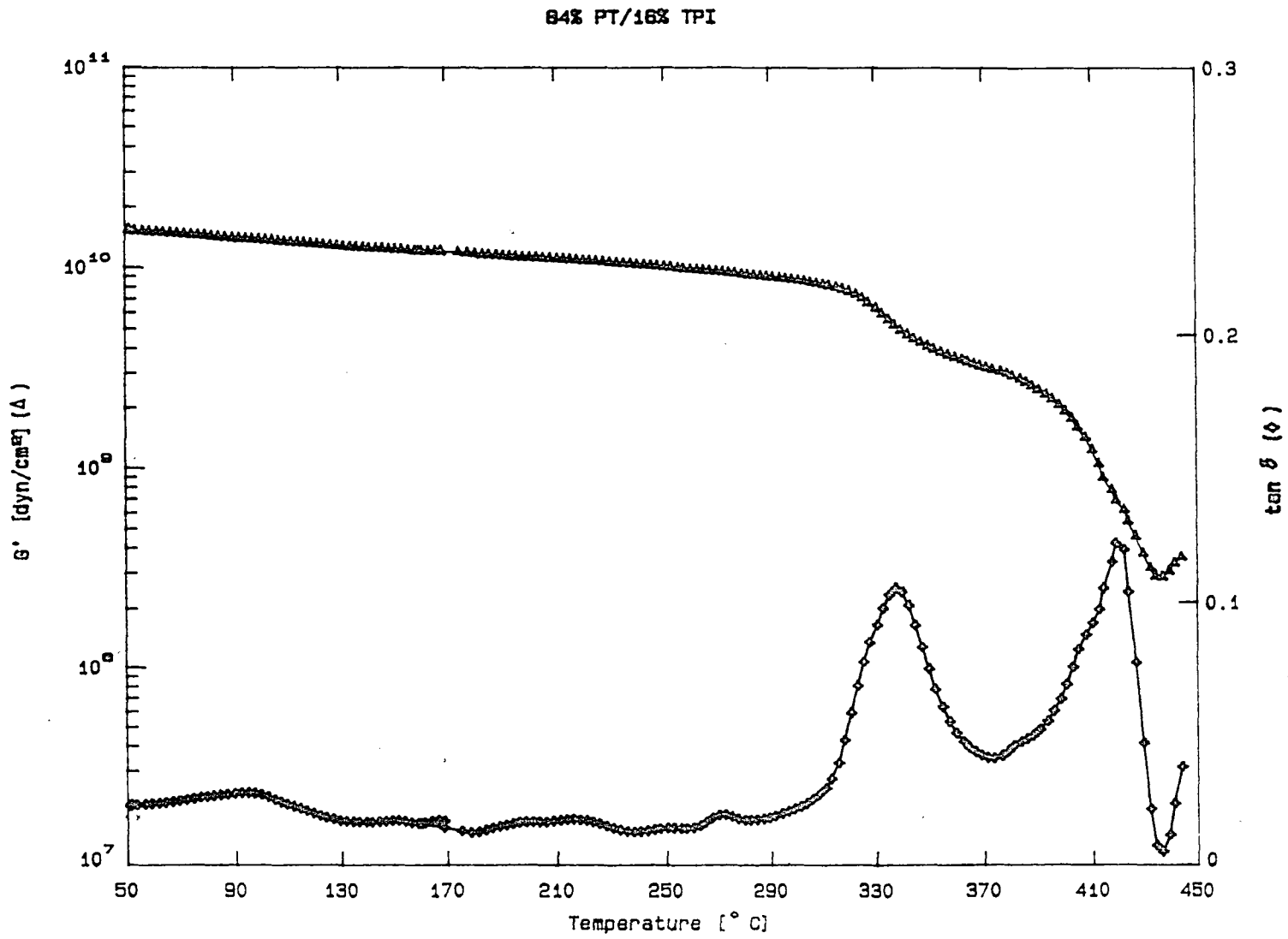
84% PT/16% TPI
G' [dyn/cm²] (Δ)
tan δ (◇)
Temperature [° C]
10¹¹
10¹⁰
10⁹
10⁸
10⁷
0.3
0.2
0.1
0
50
90
130
170
210
250
290
330
370
410
450

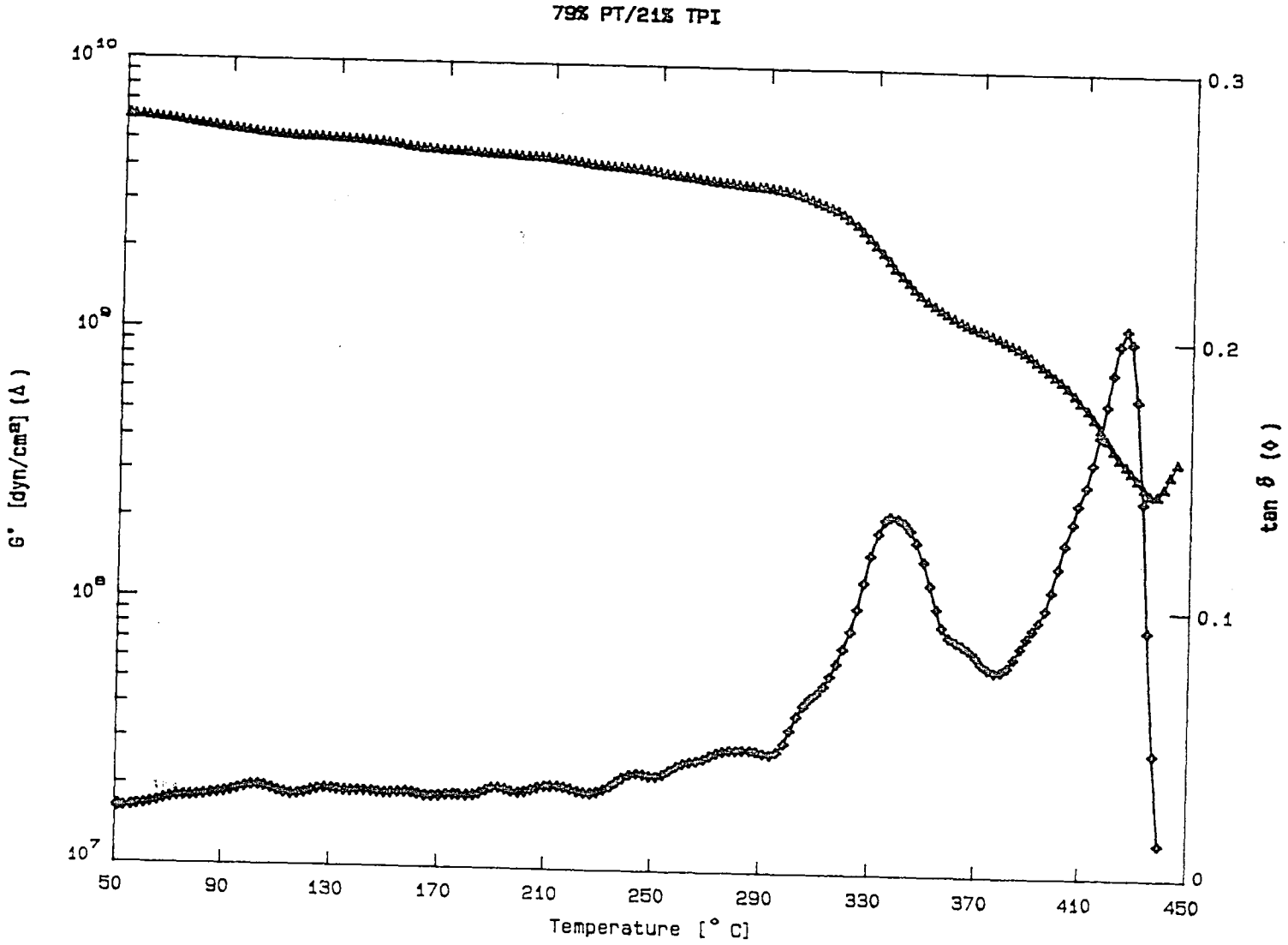
79% PT/21% TPI
10^{10}
10^{9}
10^{8}
10^{7}
G' [dyn/cm²] (Δ)
0.3
0.2
0.1
0
tan δ (◇)
50
90
130
170
210
250
290
330
370
410
450
Temperature [° C]

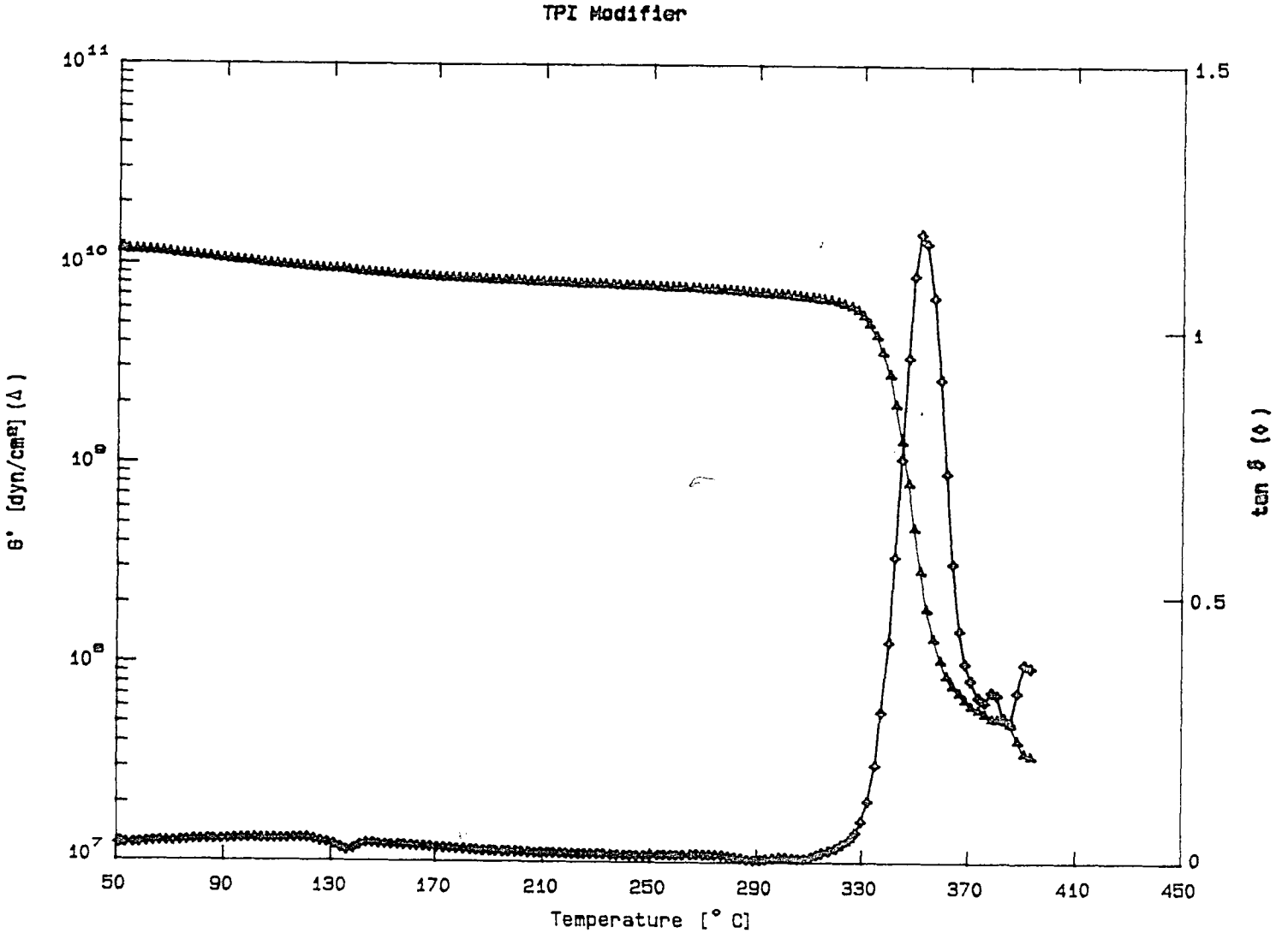
TPI Modifier
10^11
10^10
10^9
10^8
10^7
G' [dyn/cm²] (Δ)
1.5
1
0.5
0
tan δ (◇)
50
90
130
170
210
250
290
330
370
410
450
Temperature [° C]

Appendix B. Sample calculations for plane strain constraint.

In order for the mini-compact tension specimens to meet the plane strain conditions, the equations

$$t > 2.5\ (K_q/\sigma_y)^2$$

must be meet.

Since the polymers did not exhibit tensile yield, the constrain was solved for the minimum tensile yield stress that would meet the conditions of the equation given above.

Rearranging the equations gives:

$$\sigma_y > ((2.5\ K_q^2)/t)^{1/2}$$

For neat PT resin	For 79% PT/21% TPI
$K_q = 0.43$ MPa $m^{1/2}$	$K_q = 0.659$ MPa $m^{1/2}$
$t = 0.0051$ m	$t = 0.0051$ m

Therefore for plane strain to be met:

$\sigma_y > 9.5$ MPa	$\sigma_y > 14.6$ MPa

For the worst case (the toughest material), the PT/TPI blend must exhibit a tensile yield of greater than 15 MPa. It is highly unlikely that the polymers would yield at such low values, therefore the plane strain conditions were met.

Appendix C. Compact fracture toughness results for unmodified PT resin and PT/TPI blends.

Table III
Neat PT Resin

Spec #	Load (N)	a (mm)	a/W	f(a/W)	Klc
1	16.95	5.28	0.57	12.03	0.417
2	18.75	5.71	0.56	11.81	0.441
3	6.65	7.82	0.78	34.53	0.458
4	13.74	5.95	0.61	14.13	0.395
	12.01	6.47	0.66	17.84	0.435
5	22.98	4.93	0.50	9.52	0.435
				AVERAGE	0.430
				STD DEV	0.020
				cv	4.600

Table IV
95% PT / 5% TPI

Spce #	Load (N)	a (mm)	a/W	f(a/W)	Klc
1	45.77	3.41	0.33	6.12	0.549
2	31.26	4.62	0.45	8.31	0.507
3	26.00	4.03	0.40	7.31	0.483
4	39.47	3.68	0.36	6.51	0.498
				AVERAGE	0.509
				STD DEV	0.025
				cv	4.830

Table V
90% PT / 10% TPI

Spec #	Load (N)	a (mm)	a/W	f(a/W)	Klc
1	35.03	3.90	0.41	7.45	0.521
	23.55	5.18	0.54	11.10	0.522
	15.04	6.28	0.66	17.57	0.528
	7.30	7.43	0.78	35.27	0.514
2	34.72	3.94	0.42	7.63	0.535
	27.16	4.96	0.53	10.46	0.574
	7.80	7.28	0.77	33.12	0.522
3	42.50	3.29	0.37	6.69	0.592
4	53.14	2.64	0.29	5.49	0.597
				AVERAGE	0.545
				STD DEV	0.031
				cv	5.711

Table VI
84% PT / 16% TPI

Spec #	Load (N)	a (mm)	a/W	f(a/W)	Klc
1	16.61	6.20	0.66	17.47	0.597
	4.68	7.97	0.85	62.02	0.597
2	31.83	4.83	0.50	9.54	0.602
	5.81	8.05	0.83	52.05	0.599
	3.47	8.50	0.87	84.06	0.578
3	40.78	3.90	0.41	7.42	0.618
	4.70	8.05	0.84	59.60	0.572
4	52.49	3.64	0.37	6.65	0.649
				AVERAGE	0.602
				STD DEV	0.022
				cv	3.739

Table VII
79% PT / 21% TPI

Spec #	Load (N)	a (mm)	a/W	f(a/W)	Klc
1	42.59	3.98	0.42	7.73	0.661
	11.86	6.99	0.74	27.50	0.655
2	48.00	3.39	0.38	6.92	0.683
	24.40	5.15	0.58	12.52	0.629
	15.82	6.17	0.69	20.61	0.671
	8.78	6.97	0.78	35.75	0.646
3	54.76	3.27	0.35	6.41	0.705
4	7.18	7.54	0.81	43.09	0.617
				AVERAGE	0.659
				STD DEV	0.027
				cv	4.059

Appendix D. Determination of crack front radius for crack pinning model

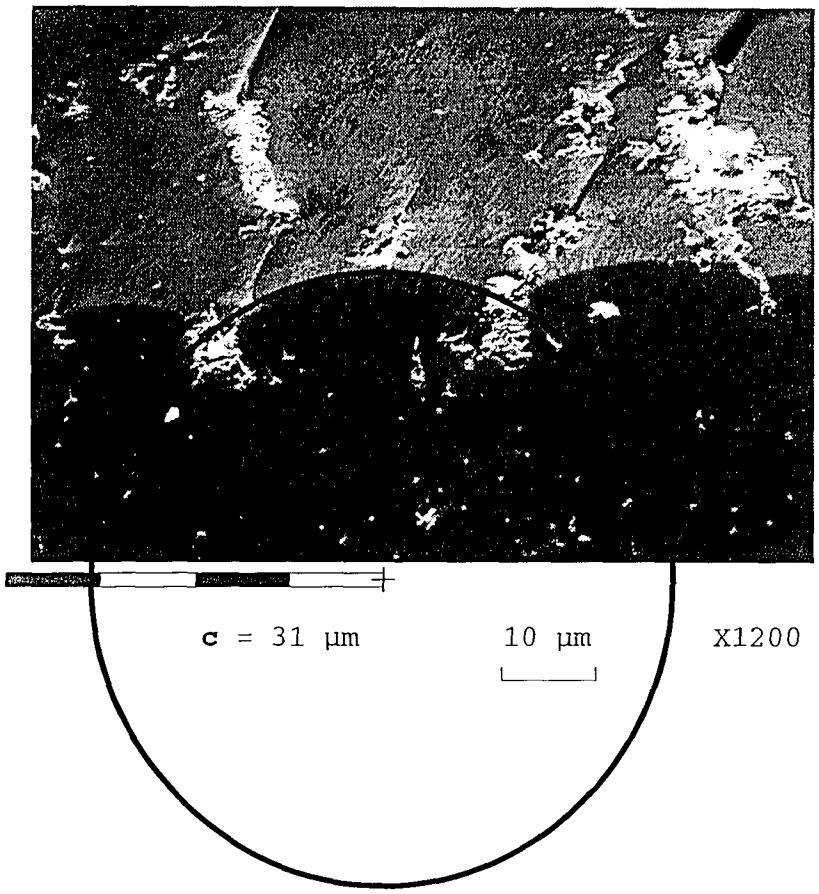

Figure 24. SEM Micrograph of 95% PT/5% TPI showing crack front radius.

Appendix D. Determination of crack front radius for crack pinning model

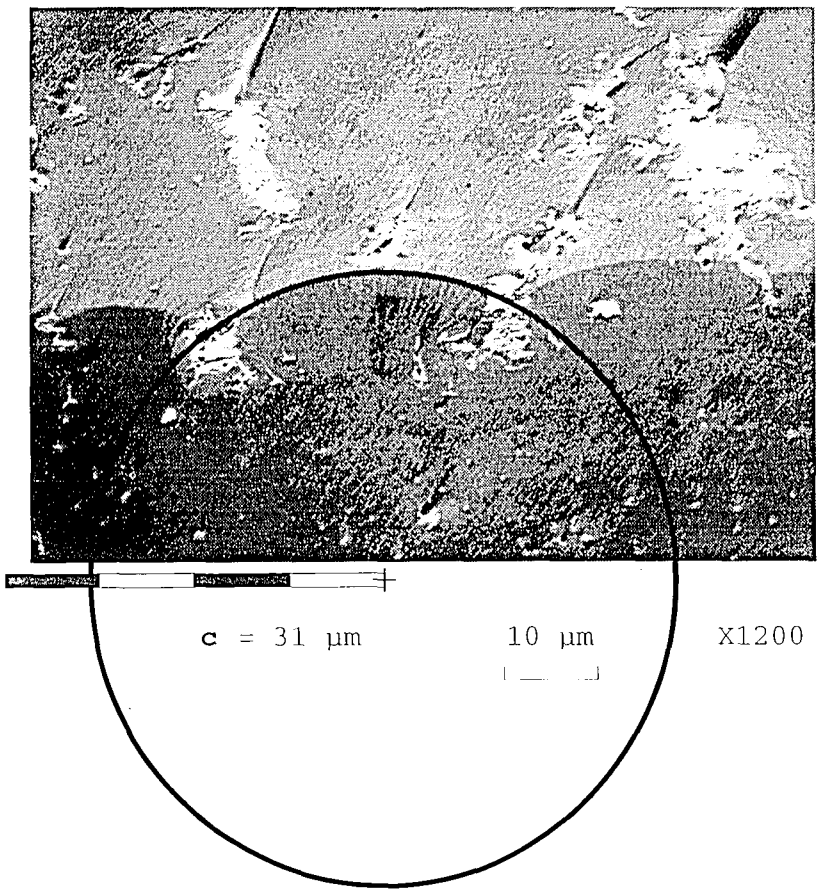

Figure 24. SEM Micrograph of 95% PT/5% TPI showing crack front radius.

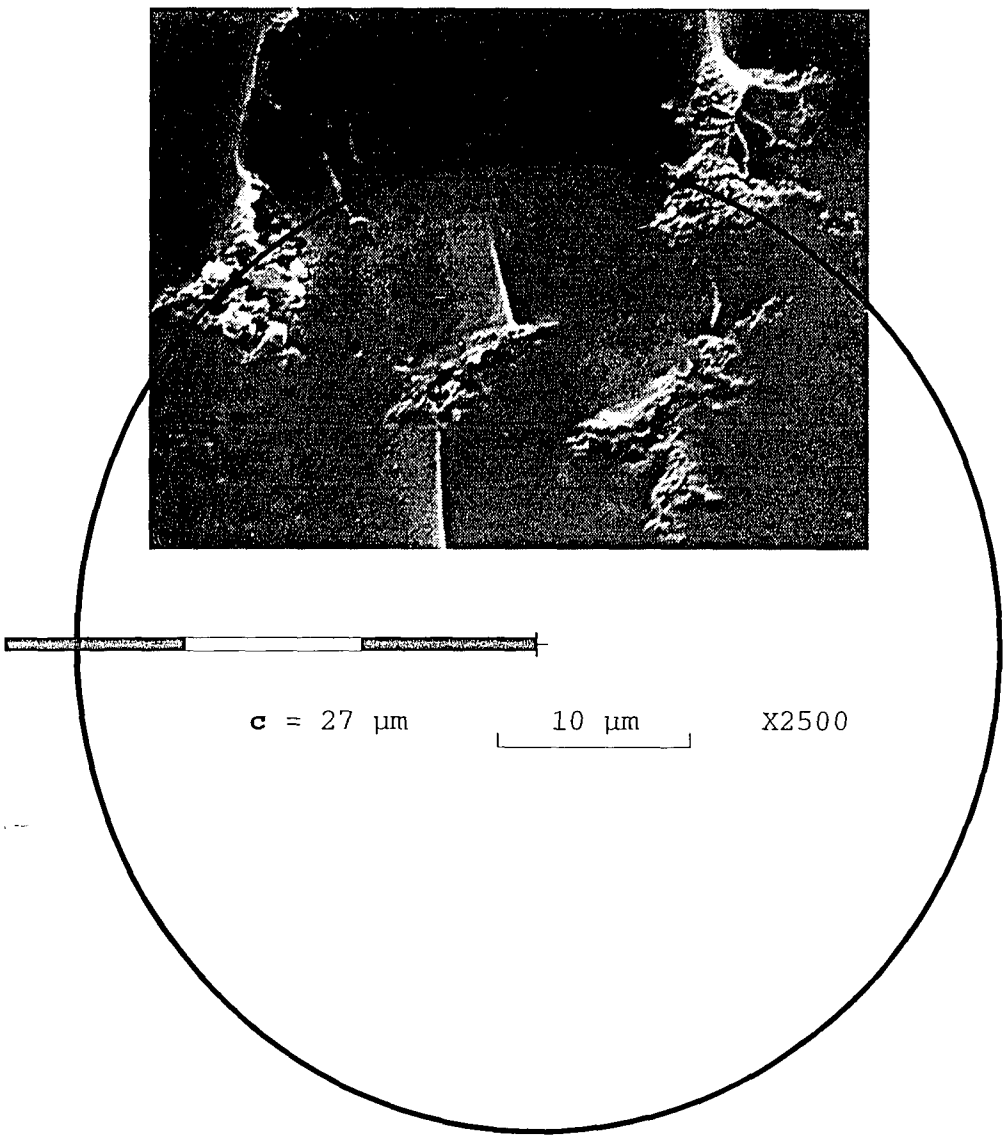

Figure 25. SEM Micrograph of 90% PT/10% TPI showing crack front radius.

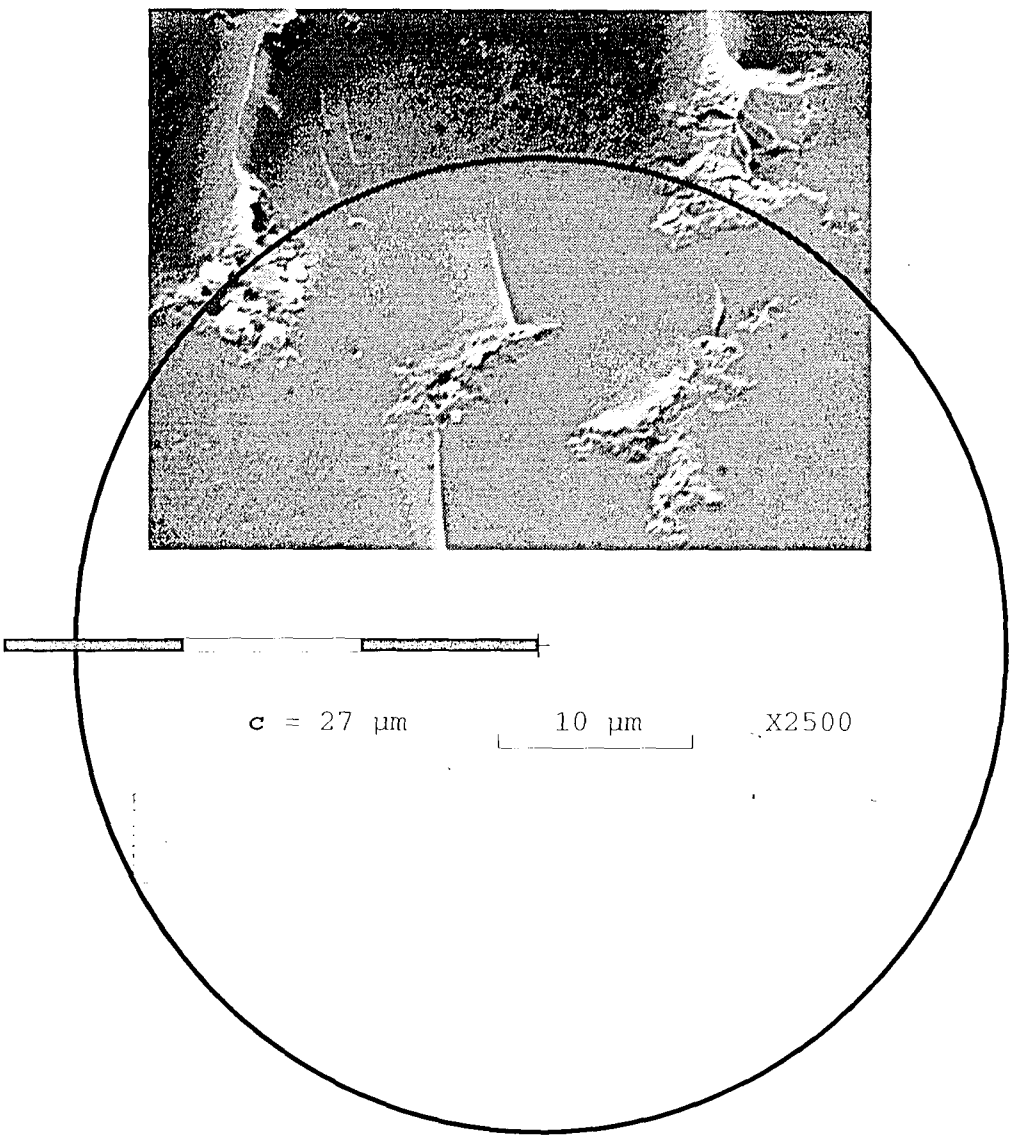

Figure 25. SEM Micrograph of 90% PT/10% TPI showing crack front radius.

Vita

Michael DiBerardino was born March 16, 1963 in Rome NY. He graduated with a degree in Chemical Engineering from Virginia Polytechnic Institute and State University in June of 1986. Mr. DiBerardino is currently employed as a Chemical Engineer in the Advanced Polymer Composite and Materials Branch at the Naval Air Warfare Center in Warminster PA.

END

OF

TITLE